University of Twente
Faculty of Engineering Technology
Department of Mechanical Engineering
Laboratory of Mechanical Automation

INFLUENCE OF AIRFLOW ON WELD DEPTH OBTAINED WITH FIBER LASER

By

Jetro K. Pocorni (s1068210)

Internship report executed from 30 August to 30 November 2011
Company : AWL-Techniek B.V.
Company Location : Harderwijk, the Netherlands
Supervisor : dr.ir. Gert-Willem Römer
Company adviser : ir. Wouter Zweers

Preface

In the second year of the master programme in mechanical engineering at the University of Twente, students are given the opportunity to apply their knowledge in a company or at a research institute.
The internship should prepare students for their future employment as leaders within an organization.
Special thanks goes to dr.ir. Gert-Willem Römer and ir. Wouter Zweers for their cooperation during this internship.

Enschede, November 2011
Jetro K. Pocorni

Abstract

During fiber Laser welding at power levels between 4-6 kW, a deeper weld was obtained if air was blown above the weld. Previous research showed that air blows away a tall heated zone above the weld. This heated zone has a low refractive index, and defocuses the Laser beam.
In this report the weld depth was measured as a function of different air velocities ranging from 0-35 m/s; the corresponding air consumption was also noted. The measurements were done by positioning a nozzle at various heights. Also, multiple nozzles were stacked above each other to form a tall air profile. Air was blown perpendicular and parallel to (opposite to and in the same direction as) the weld direction.
The weld depths increased up to 2 mm while air was blown above the weld.
The application of air enables deeper welds while maintaining the same Laser power. Thus, for a deeper weld, the weld speed can be increased and productivity improved.

Keywords: fiber Laser, welding, refractive index of air, productivity in Laser welding

Nomenclature

d_{max}	: Maximum weld depth
d_0	: Weld depth at zero air velocity
d	: Weld depth
D_o	: Diameter of transport fiber
$F_{focusing\ lens}$	: Focus length of focusing lens
$F_{collimator}$	: Focus length of collimator
h	: Height of nozzle above test piece
P	: Laser power
V_{air}	: Air speed above weld
V_{Laser}	: Weld speed
q_{air}	: Volumetric flow rate (air consumption)
w	: Width of weld

Table of contents

1 Introduction

AWL-Techniek B.V. is located in Harderwijk, the Netherlands. AWL is a system integrator which manufactures automated machines for welding and cold-joining applications.
The integration of Lasers in AWL's machines started in 2003, and in the meantime Laser welding has taken up more than 60% of the turnover.

AWL noticed that welding non galvanized steel with 4-6 kW fiber Lasers led to deeper welds if an airflow was blown above the weld.
The purpose of this report is to find the reason for the increased weld depth while blowing air and experimentally determine the optimal amount of air needed to obtain deeper welds.

1.1 Problem definition

The application of air while welding with a fiber Laser enables deeper welds while maintaining the same Laser power. Thus, the weld speed can be increased and productivity improved, which is an economic advantage.

If the airflow above the weld is weak, the plume above the weld is not blown away, and the weld depth is observed to be less deep. On the other hand, a strong airflow blows the molten material out of the weld. So, the airflow should lie between these two extremes, but the amount of air used should be as minimal as possible since the compression of air costs energy.
This leads to the definition of the following research questions:

1. What is the optimal amount of air needed to obtain deeper welds?
2. How should this airflow be directed compared to the welding direction?

Besides these two research question, the following sub question should be answered:

Should the airflow be blown directly above the weld or should this be done throughout the whole cell?

1.2 Structure of report

First, in chapter 2, background information is given on the effect of applying air during Laser welding. Previous research done on the subject is also summarized. In chapter 3 the experimental setup for the measurements is described. Each measurement device is explained briefly, and the procedure by which measurements were carried out is explained. Chapter 4 deals with the analysis of measurement results. Different cases are specified and the results from these cases are compared with each other. The report is completed with conclusions concerning the experiments. Some recommendations for further research and experiments are also given.

2 Theory

In general, components that build up air such as Nitrogen, Oxygen and water vapor have a negative effect on the material being Laser processed i.e. nitrides, oxides and pores are formed in welds and give rise to deficient mechanical properties [1].

In traditional arc welding the melt pool is shielded against the ambient air by inert gasses such as Helium and Argon. Nowadays, air is applied as a highly effective or at least acceptable shielding gas while steel is Laser welded [1].
The following reasons are behind the acceptance of air as a reasonably effective shielding gas [1]:

- The width of welds that are formed with Laser is small since, depending on the optics, the diameter in the focus can be made very small i.e. between 100-800 μm. Thus, the area exposed to ambient air is minimal.
- Laser welding is done at high speed; consequently the exposure time the melt pool has with ambient air is short.
- Since the plasma temperature for CO_2 Lasers is higher than for fiber Lasers, the amount of activation energy available for oxidation while welding with a fiber Laser, is smaller.

The coefficient of inverse Bremsstrahlung absorption takes energy from the incident Laser beam and redirects it into heating of the plume. This coefficient is a factor 100 lower than that of the CO_2 Laser [4, 6]. Thus, the absorption of fiber Laser radiation by the plume is far less in comparison with the CO_2 Laser, and the chance of plasma formation decreases.

Even if there is little or no plasma while using the fiber Laser, there is still a plume above the weld. This plume also attenuates the Laser power by scattering the Laser radiation [4]. Depending on the size of the vaporized metal particles, the scattering can be classified as
- Rayleigh scattering: particles are small compared to the Laser wavelength, or
- Mie Scattering: particle size is approximately the same as the Laser wavelength [7].

Since it is proven that the negative effect of air on the melt pool is limited, air itself can be used to blow the Laser-induced plume away. The purpose of air is not as a traditional shielding gas (since the blowing air is not used to shield the melt pool against foreign gasses), rather the blowing air should keep the atmosphere above the weld pool fresh.

2.1 Previous research on the influence of air

In [2,3] research is done on the influence of the atmosphere on the penetration depth. The setup used during this research is displayed in Figure 1, and the specifications of the Lasers used are given in Table 1.

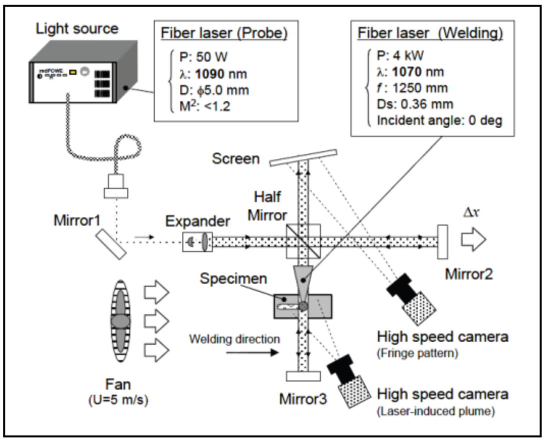

Figure 1 Experimental setup [2].

Laser Power, P	4 kW
Welding speed, v	5 m/min
Defocussed distance, f_d	0 mm
Weld length	175 mm
Probe Laser power, P_p	50 W
Test piece material	Zink coated steel

Table 1 Experiment specifications [2].

In Figure 1 a probe Laser, Michelson interferometer (consisting of a half mirror, mirror 2 and 3 and screen) and high speed camera are used to visualise fringe patterns that are the consequence of the atmosphere above the melt pool. A second high speed camera is used to capture the behaviour of the fiber Laser-induced plume. Also, a fan is used to study the effect of blowing air while welding.

In Figure 2 the diameter of the fiber Laser beam is plotted against the distance from the focus instantly after irradation, and after 15 minutes of irradation. The focus shift of 3 mm is, at first thought, attributed to the thermal lens effect that causes the lense to deform in such a way that the focus length changes. But this focus shift is very small compared to the focus length of the lens i.e. 1250 mm, so the thermal lens effect is dismissed as the cause.

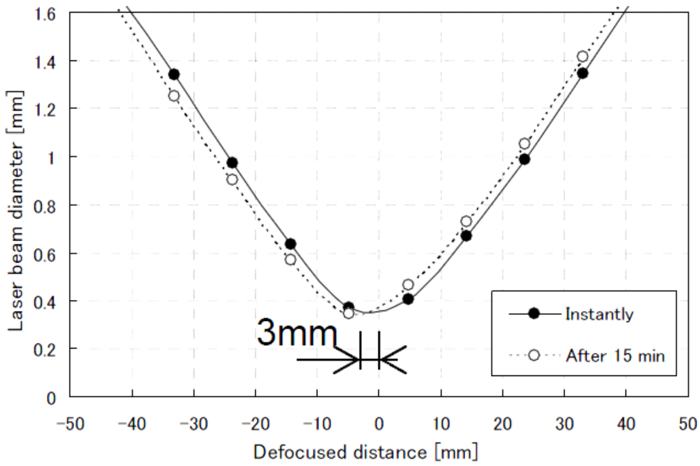

Figure 2 Beam diameters instantly after irradation, and after 15 min. of irradiation [2].

In Figure 3 and Figure 4 the weld seam at the top and bottom surfaces of two test pieces are displayed. Both experiments are based on the welding parameters in Table 1. Between the instant of time t_2 and t_3, the penetration depth of the weld decreases; there is a transition from full penetration to partial penetration.

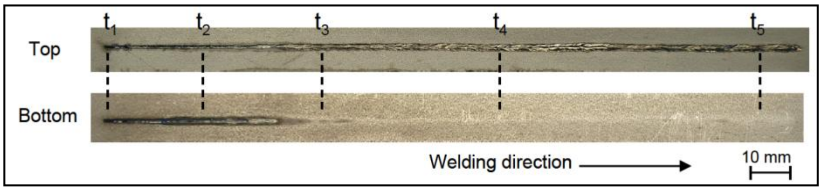

Figure 3 Top and bottom appearance of weld with fan off [3]. See Table 1 for Laser specifications.

In Figure 4 the weld seam is displayed if the fan is turned on with an air speed of 5 m/s. The bottom weld seam shows that the test piece is fully penetrated over the whole length.

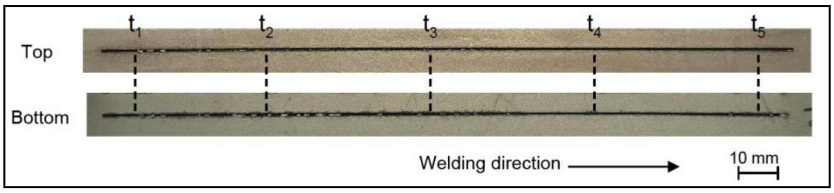

Figure 4 Top and bottom appearance of weld with fan on [3]. See Table 1 for Laser specifications.

Since the thermal lens effect is rejected as the cause of the focus shift, and the plume is assumed not to absorb Laser radiation at 1070 nm, other causes must be considered. In Figure 5 (a) the Laser-induced plume is visualized together with the fringe pattern that is a consequence of the atmosphere above the melt pool.

The interferometer displayed in Figure 1 consists of a half mirror that splits the probe light into two separate yet identical beams. One beam travels through the atmosphere above weld pool while the other beam travels on a path without any obstacle and is used as a reference. After reflecting on mirror 2 and 3, the same half mirror combines both beams and projects them onto a screen. The projection is then captured with a high speed camera and is called a fringe pattern.
Since the probe light is an electromagnetic wave, the superposition of the two beams is also a wave. The black and white stripes represent the extrema of the superposed wave [8]. Where the stripes are (nearly) horizontal, there is no or little difference between the beam's paths. But where the stripes are curved, there is a phase difference between the two beams [3]. This is caused by the difference in refractive index in the beam's paths.
The curved patterns are formed in the region around the plume, and this region is called the low refractive index zone [2, 3]. This low refractive index zone is a consequence of spatially heated air around the plume [3].

When the fan is turned on in Figure 5 (a) and (b), the plume is partially blown away and the region with curved fringe pattern becomes smaller, and shifts to the right.

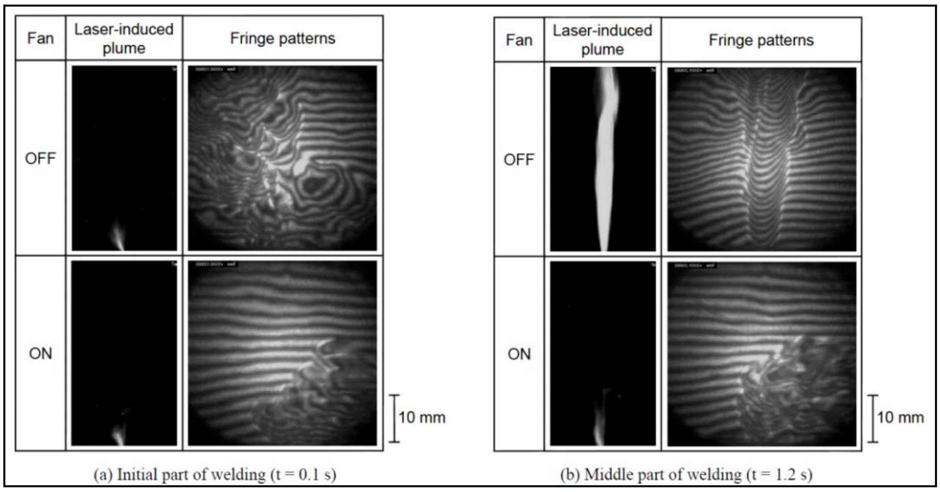

Figure 5 Plume and fringe pattern at (a) t=0.1 s and (b) t=1.2 s.[2]. Welding parameters given in Table 1.

In [2] the height of the low refractive index zone exceeded 400 mm while the height of the plume was measured to be 100 mm. So, this refractive zone can be a factor 4 taller than the Laser-induced plume.
In Figure 6 the plume, fringe patterns and test piece surface are shown as a function of time while the fan is off. The fringe patterns show that low refractive index zone encloses the plume, and at t_2 the zone is far larger than the plume.

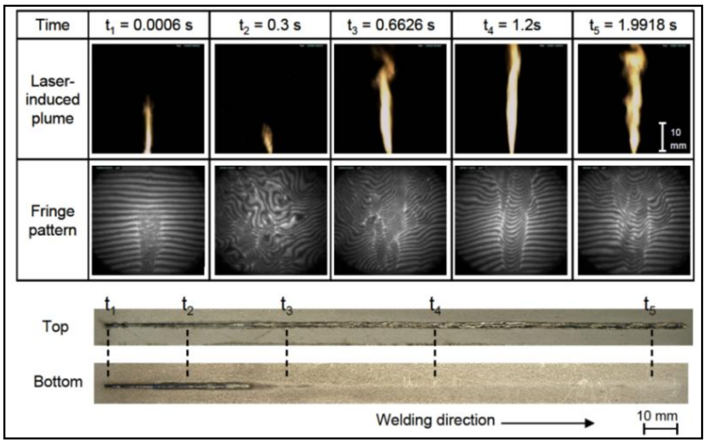

Figure 6 Plume, fringe patterns and weld appearances at different instances of time (fan turned off) [3]. Welding parameters given in Table 1.

If the fan is turned on, the plume height is lower, and the low refractive index zone decreases in size and shifts to the right in the direction of the blowing fan. So, the Laser beam is able to reach the test piece surface with fewer interruptions.

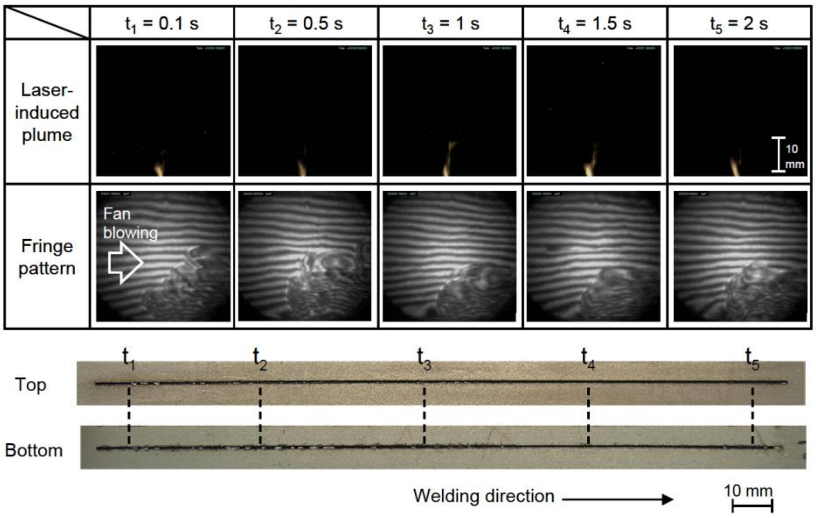

Figure 7 Plume, fringe patterns and weld appearances at different instances of time (fan turned on) [3]. Welding parameters given in Table 1.

This low refractive index zone defocuses and refracts the fiber Laser beam and has been proven to be transmissive: In [2], the brightness of the probe Laser is also investigated; the brightness does not decrease after going through the atmosphere above the weld pool, so the atmosphere consisting of the low refractive index zone and the plume, does not absorb radiation energy. This is an expected result because of the coefficient of inverse Bremsstrahlung absorption. Thus, the fiber Laser radiation is merely defocused and refracted.
Rayleigh scattering is also considered the cause of refraction of the Laser beam [4].

Figure 8 shows the distribution of the refractive index of air along the beam axis. The refractive index is smallest at the center of the beam (Radius= 0 mm), and decreases with height.

If the power density distribution of the Laser beam is Gaussian, the beam will refract most where its intensity is highest.

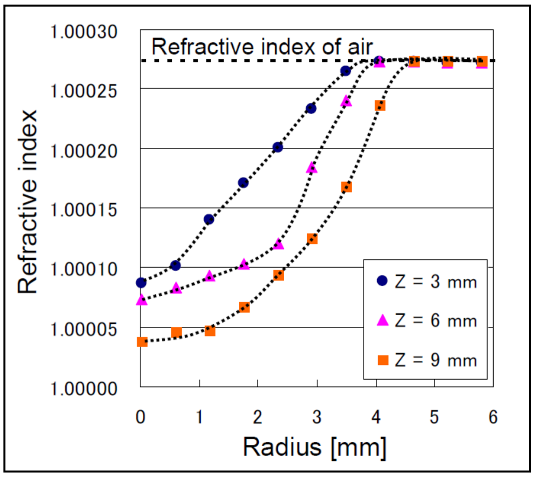

Figure 8 Distribution of refractive index along the beam radius at different heights measured from the specimen's surface [3]. This figure is based on 30 ms pulsed YAG Laser.

2.2 Concluding remarks and prospect on experiments

The following conclusions and prospects follow from literature research:

- The research done in [2, 3] indicates that the low refractive index zone is the leading cause for attenuation of the Laser power density reaching the test piece surface. This result is somewhat surprising, and has just recently been published. Heating of the air during welding is actually an expected result, but its significant effect on the weld is quite peculiar. Research on the low refractive index zone was first published in 2008.

- The background information provided in this section proves that the atmosphere above the weld pool must be kept fresh in order to obtain deeper welds.

- Since the height of the low reflective index zone can be tall, experiments must be done by placing an air nozzle at different heights.

- Also, a set of nozzles will be aligned above each other to blow air along the whole height between the Laser optical head and test piece surface.

- The low refractive index zone is a localized zone, so it is not required to blow air throughout the whole cell.

- In [2] and [3] experiments are done with an air velocity of 5 m/s, as a guideline the experiments in this report started at low velocities around 1 m/s.

- Figure 6 shows that some time passes before the low refractive index zone has grown and distribute itself. Thus, the weld cross section should be taken at some length from the beginning of the weld.

3 Experimental setup and procedure

On the basis of the background information in chapter 2, experiments were conducted by using pressurized air to blow away the low reflective index zone above the weld. First, experiments with one nozzle were carried out, followed by experiments with an array of nozzles placed above each other. The following experiments were done by using a single nozzle:

- the airflow is perpendicular to the weld direction
- the airflow is parallel to the weld direction, yet in the same direction
- the airflow is parallel and opposite to the weld direction.

During the second part of the experiments, the nozzles were aligned above each other in such a way that the space between the optical head and the test piece surface was constantly kept fresh during welding. Based on the results with one nozzle, further experiments were carried out with an array of nozzles. All experiments are carried out in AWL's robot welding test cell.

3.1 Setup with one nozzle

In Figure 9 and Figure 10 the experimental setup is shown. Compressed air with a peak pressure of 7 bar was used during the measurements. A control valve regulated the air velocity and volumetric flow rate in the ducts. The measurements for the volumetric flow rate were done with a Festo SFAM-62 flow sensor. The flow sensor had an accuracy of $3\% \cdot 5000 \frac{\mathrm{l}}{\mathrm{min}} = 150 \frac{\mathrm{l}}{\mathrm{min}}$ (Appendix 2.2). The pressure was measured with a Festo SPAB-P10R pressure sensor with an accuracy of $2\% \cdot 10\ \mathrm{bar} = 0.2\ \mathrm{bar}$ (Appendix 2.3).
A Silvent 961 nozzle was used to distribute the air in a broad but thin air cone. The air speed above the test pieces was measured by using a Höntzsch anemometer with an uncertainty of $2\% \cdot \text{measured value} + 0.02 \frac{m}{s}$. The anemometer measured the speed for 30 sec. and determined the average velocity (Appendix 2.8).

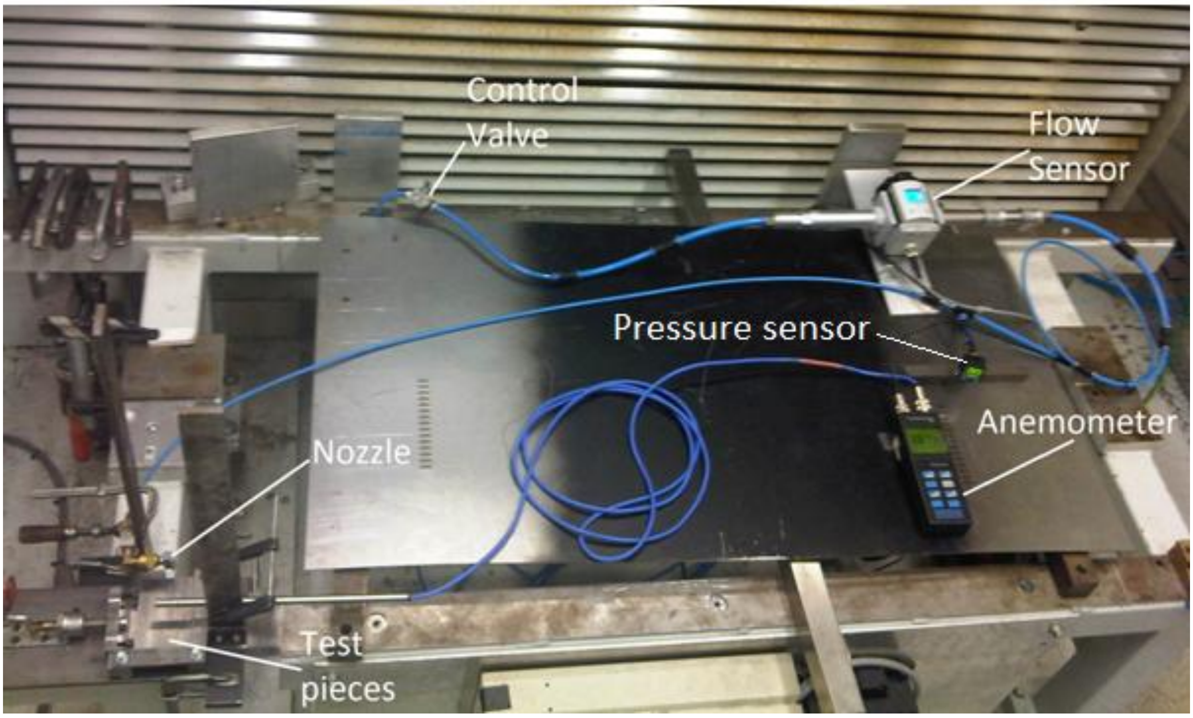

Figure 9 Experimental setup.

A 6 kW Ytterbium fiber Laser (IPG YLS 6000, Appendix 2.5) was used with a 200 µm diameter transport fiber. A Precitec optical focusing head consisting of a collimator with a focus length of 150 mm and a focusing lens with a focus of 485 mm, focused the Laser radiation on the test piece.
Thus, the spot diameter on the test piece equaled:

$$(3.1) \qquad \left(\frac{f_{focusing\ lens}}{f_{collimator}}\right) \cdot D_o = 647.7\ \mu m$$

All measurements in this report were done in focus. Figure 10 displays the optical head and the industrial robot.

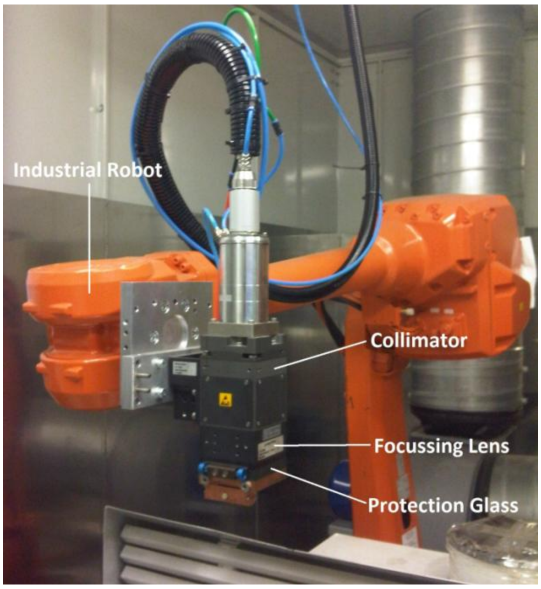

Figure 10 The optical head and industrial robot.

The optical head was connected to a 6 axis ABB IRB 4600 robot which enabled movement of the optical head.
Before each experiment, the power of the Laser radiation out of the optical head was measured using a Laser power meter (Primes PocketMonitor 70 icu). In Figure 11 the power meter is displayed. The accuracy of the power meter was ± 4% of the measured value (Appendix 2.6).

Figure 11 Application of the Laser power meter.

Two stands were designed and created as supports for the anemometer sensor and for the nozzle. Figure 12 displays a close up of the stands and other components. The upper stand has a height of 475 mm while the lower stand has a shorter height of 445 mm. Both stands are on different platforms, and their heights are chosen such that there is no collision with the optical head.
The stands were created by screwing together two St 37k steel beams with cross section of 30 x 6 mm. Clamp tools were used to fasten the nozzles and anemometer sensor to the stands, as is shown in Figure 12. The clamps also allow the height of the nozzles to be easily varied.

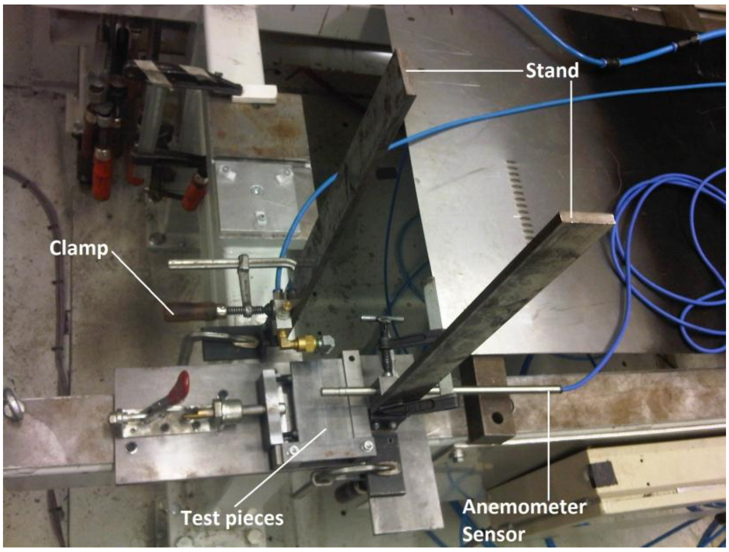

Figure 12 Close up of experimental setup

The test pieces were all made of cold worked St 37k steel and were welded together by creating horizontal welds. Each weld represented a different parameter. In Figure 13 (a) a top view of the welded test pieces is shown.
The weld speed was chosen equal to 80 mm/sec. and the weld length was 20 mm. These values for the speed and weld length were chosen because they are often used in applications of AWL.

After the test pieces were welded, they were taken apart and the cross section was grinded, polished and finally etched with a solution of alcohol and Nitric acid. Figure 13 (b) displays a cross section of the test pieces; the upper test piece was obtained without any surface treatment and the lower cross section was obtained after grinding, polishing and etching.
Lastly, the intersection of the welds was studied by photographing them with a Novex RZ microscope (Appendix 2.7). The width and depth of the welds were taken from these photographs. Technical information concerning each of the devices mentioned so far is given in Appendix 2.

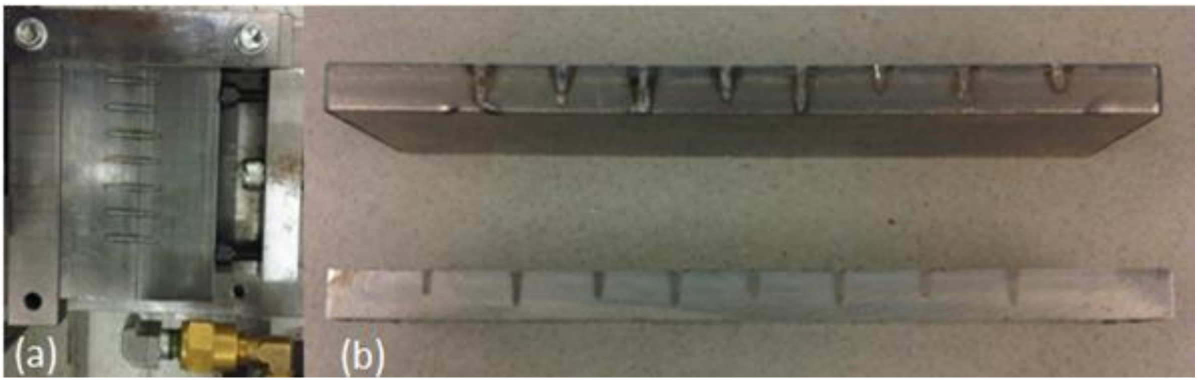

Figure 13 (a) Top view of the welded test pieces, and (b) cross section of the test pieces.

3.2 Setup with an array of nozzles

Six nozzles were placed above each other to blow the low refractive index zone away. An amount of six nozzles was chosen because of the availability of stock nozzles within AWL. The same stands, as in the one nozzle case, were used. The nozzles were fastened to the stand with clamp tools, as is displayed in Figure 15. The other stand was used to support the anemometer sensor. The full setup is displayed in Figure 14. Each nozzle received compressed air by using a manifold. An experiment was also done to find out if an equal amount of air was fed to each nozzle by the manifold.

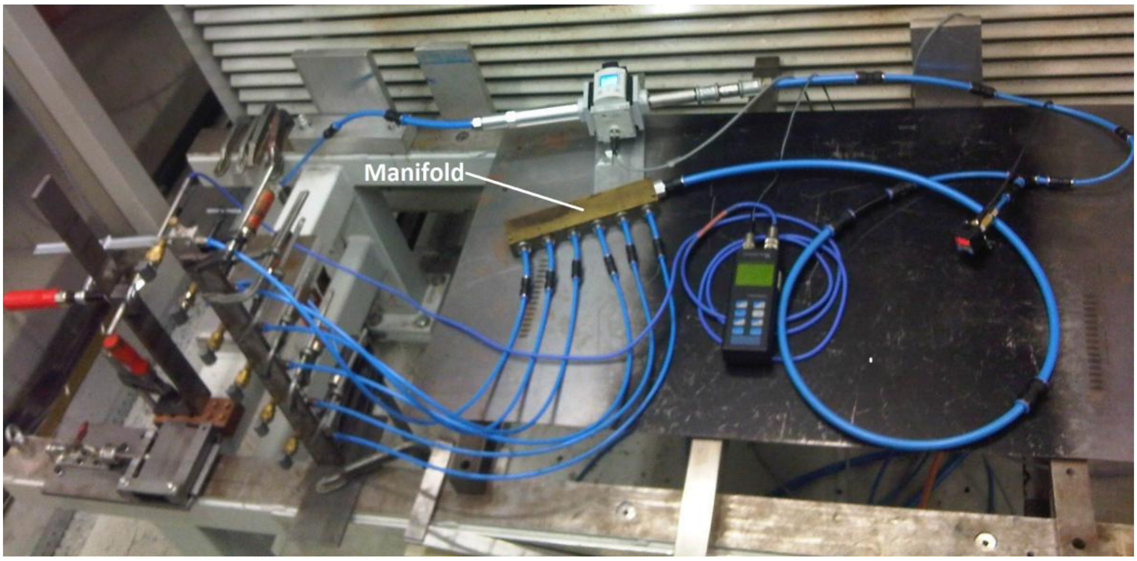

Figure 14 Experimental setup with six nozzles.

Because of the geometry of the clamp table and the height of the stand (Figure 15), the nozzles were placed at 80 mm center to center distance above each other. Each nozzle has a height of 24 mm. The total height that was kept fresh with air, including the height of the nozzles, equaled 424 mm while the focus was 485 mm. Thus, only 61 mm was not kept fresh. The largest portion of this 61 mm consisted of a safety margin that should prevent collision with the optical head.

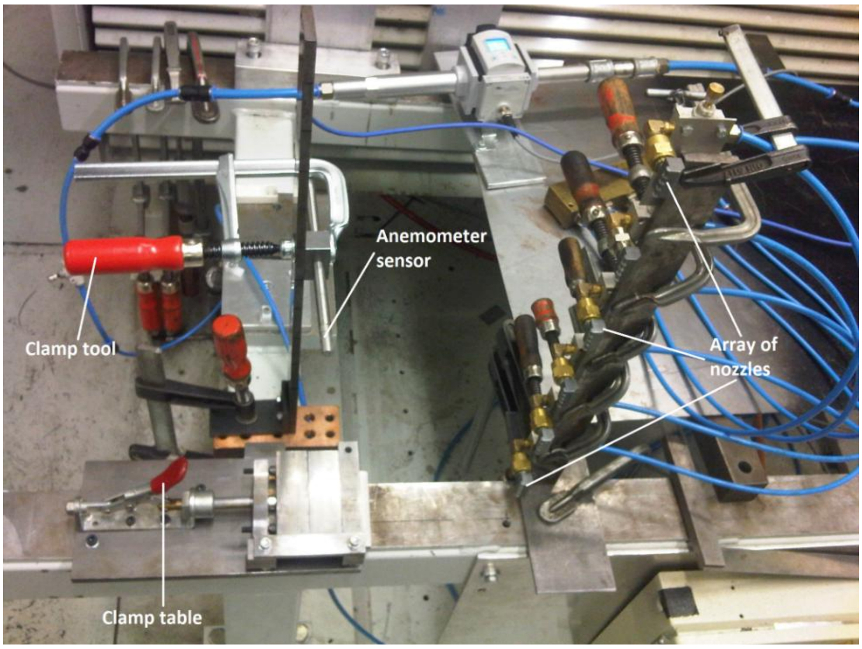

Figure 15 Close up of setup.

The measurements were carried out by controlling the flow rate and setting it to certain a value with the control valve. The velocities in the air profile above the weld were measured at various heights with the anemometer i.e. 11 air measurements were done in the air profile above the weld. Six measurements were done at the height of the center of the nozzle and five measurements were done at a height in between the nozzles. Lastly, the mean of these velocities was determined to obtain a univocal velocity.

3.3 Air distribution per nozzle

To check whether an equal amount of air was fed to all six nozzles, the pressure in each of the six tubes that led to the nozzles was measured. The volumetric flow was set to 151 l/min. during these measurements. Below table displays the pressure in each tube; the tube numbering increases from the bottom nozzle up (see Table 2 and Figure 16).

Tube	P (bar)
1	0.22
2	0.23
3	0.23
4	0.23
5	0.23
6	0.23

Table 2 The pressure in the tubes.

Tube 2-6 had the same pressure while tube 1 had a different pressure that only differs 0.01 bar. Since the difference was this small, it was assumed that each nozzle received the same amount of air. The pressure in the main tube equaled 0.34 bar, so there is some pressure drop in the tubes and manifold. Yet the distribution to each nozzle is approximately the same.

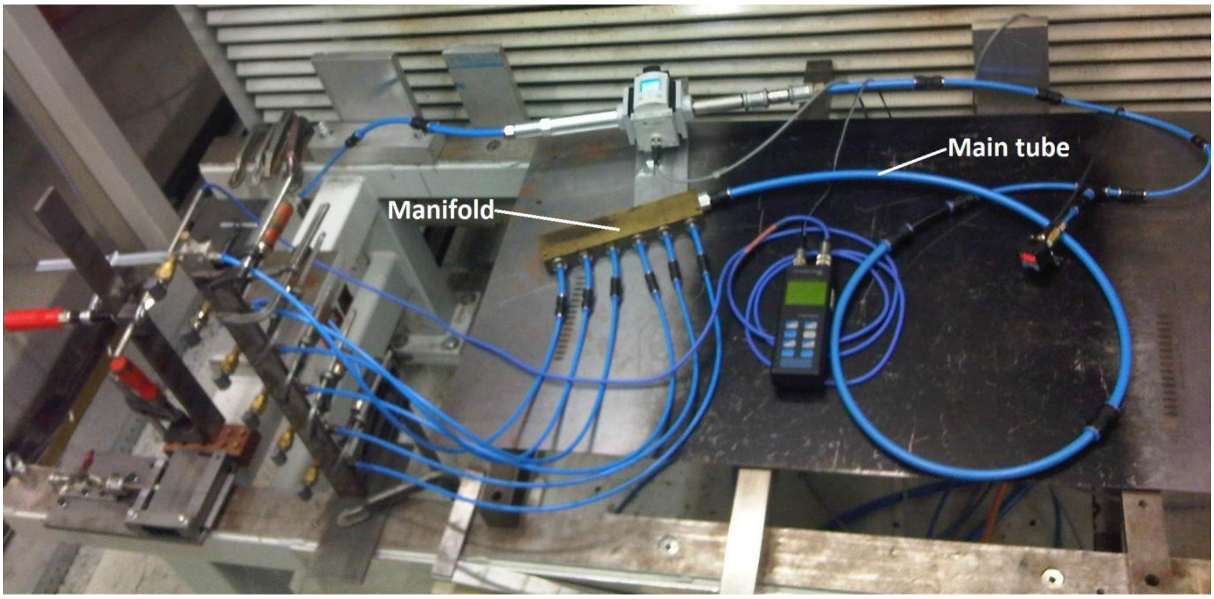

Figure 16 The experimental setup with the main tube, manifold and six nozzles.

4 Experimental results and analysis

The first experiments were carried out at 1 kW, but the welds were shallow and barely visible under the microscope. Thus, the depth measurements could not be done very accurately. Figure 17 gives an impression of such a weld made at 1 kW.

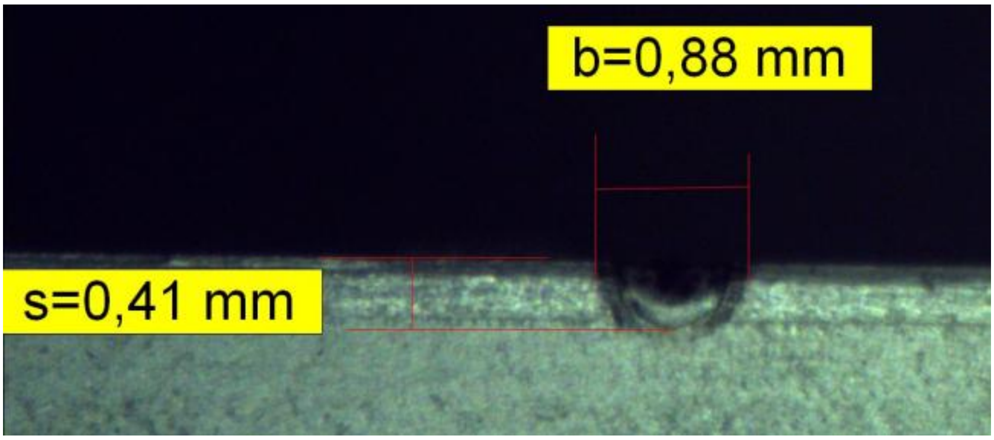

Figure 17 Shallow weld made at 1 kW and V_{air} = 0 m/s.

4.1 Application of one nozzle at low air velocity

In order to obtain more visible welds, the Laser power was increased to 2 kW. During these experiments, air was blown perpendicular to the weld direction. The air velocity was kept low between 0-6 m/s since previous research in [2] and [3] was carried out at low speed.
The height of the nozzle above the test piece surface was varied between 0-30 mm with steps of 10 mm. For each nozzle height, several welds were made on the test pieces; each weld was made with a different air speed. The air speed was varied between 0-7 m/s with steps of 1 m/s. The results for these experiments are given in Figure 18.

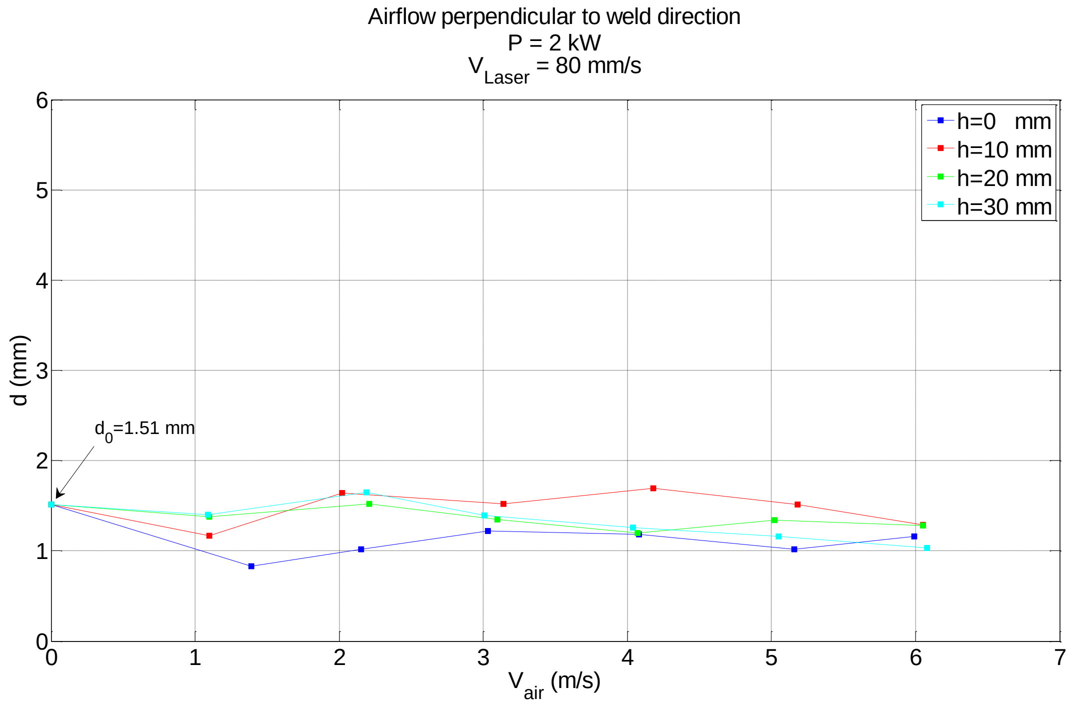

Figure 18 Weld depth vs. air speed while airflow was perpendicular to weld direction.

Figure 18 shows that the positioning of the nozzle right above the test pieces (h = 0 mm) gives the worst results regarding the weld depth. This is expected since the blowing air interacts with the melt pool.
An example of the influence air has on the appearance of the melt pool is given in Figure 19 i.e. the upper weld displays a melt pool obtained at zero air velocity while the lower weld displays a melt pool obtained with blowing air. The upper melt pool has sharp edges while the lower melt pool has ripples, and the edges of the melt pool are rounded off.

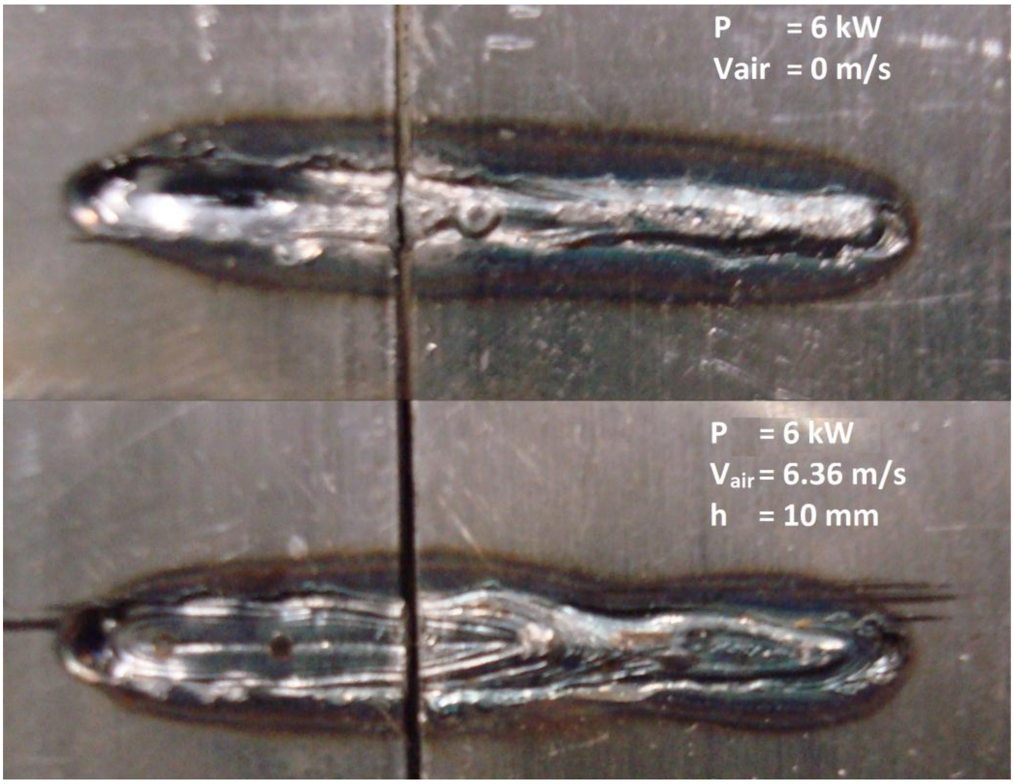

Figure 19 Influence of air on weld pool. Both welds were created by welding from right to left; the airflow was also blown form right to left using one nozzle.

Figure 18 also indicates that the blowing air does not increase the weld depth significantly at low Laser power and low air velocity i.e. the depth seems to have a constant trend. Other experiments at 2 kW, such as varying the air direction, were halted in order to proceed at higher Laser power i.e. 4 kW. The results at 4 kW are displayed in Figure 20, Figure 21 and Figure 22. Each figure depicts a case in which air is blown perpendicular, opposite and in the same direction as the weld direction.

At each power level (2, 4 and 6 kW) several measurements of the weld depth at zero air velocity were carried out. To have a univocal depth at V_{air}= 0 m/s, the mean depth was taken and the result is consistently presented in all graphs displaying the weld depth versus the air velocity.

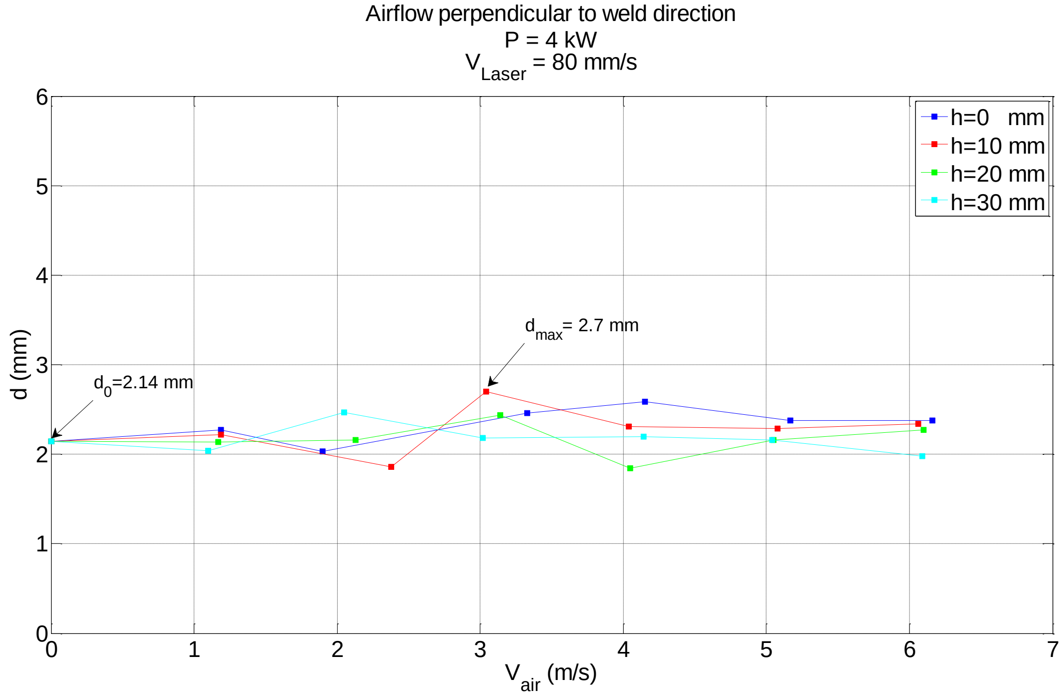

Figure 20 Weld depth vs. airspeed at 4 kW while airflow was perpendicular to weld direction.

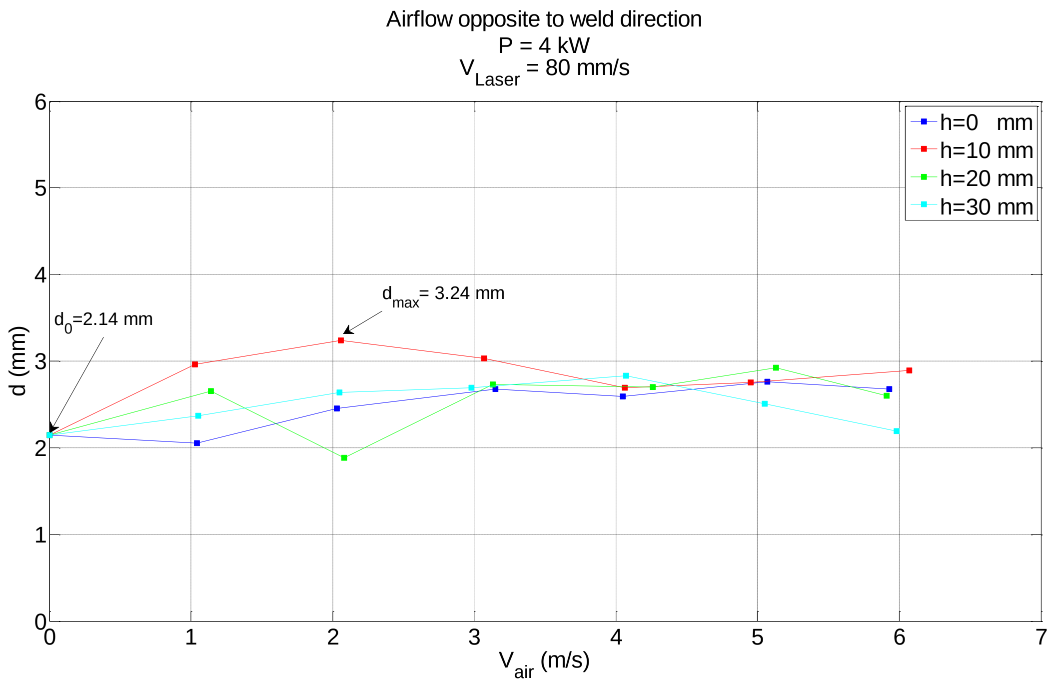

Figure 21 Weld depth vs. airspeed at Laser power of 4 kW while airflow was opposite to weld direction.

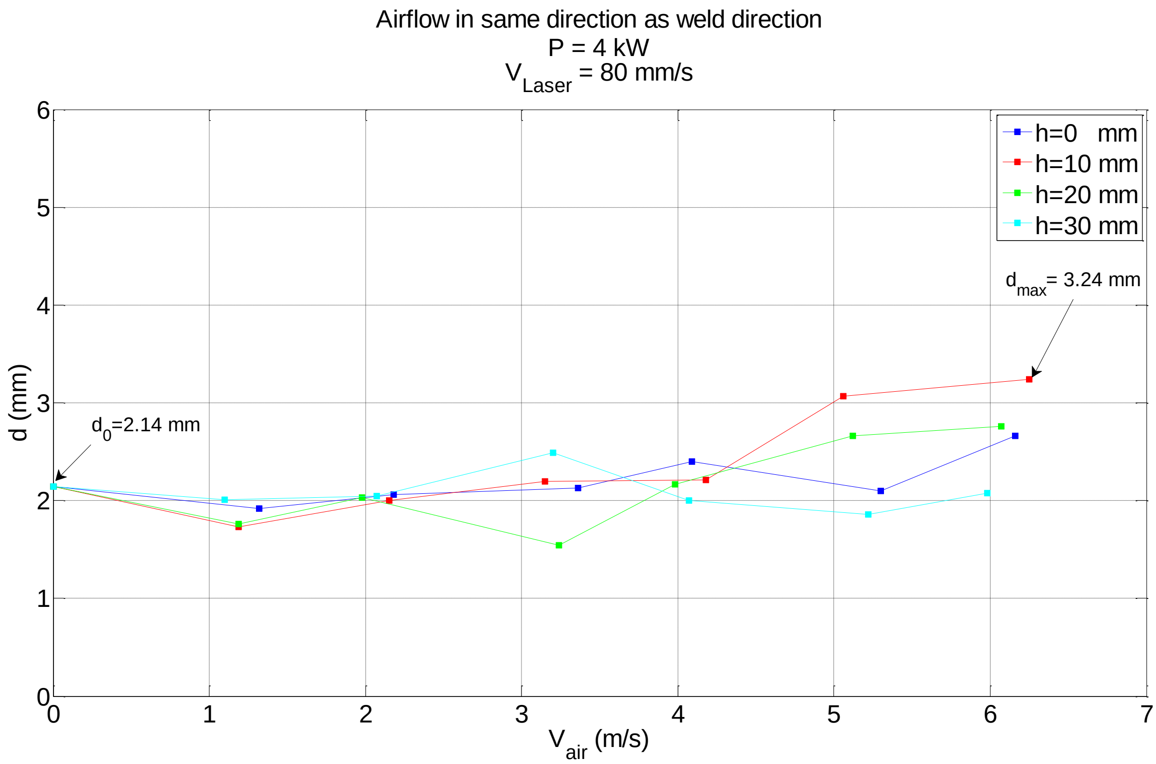

Figure 22 Weld depth vs. airspeed at 4 kW while airflow was in the same direction as weld direction.

The deepest welds were obtained when the nozzle was positioned at 10 mm height from the test piece surface and when the air direction was parallel (opposite or same direction) to the weld direction. Noteworthy is what happens when air is blown perpendicular: the maximum weld depth is smaller than when air is blown parallel.

Figure 20, Figure 21 and Figure 22 show that positioning of the nozzle right above the weld (h= 0 mm) leads to reasonable results, but not the deepest welds.

The experiments suggest that a higher airspeed would produce deeper welds; this will be investigated in the next experiments.

4.2 Application of one nozzle at high air velocity

The results obtained so far suggest that further tests should be done at higher air velocities and at a nozzle height of 10 mm.
The maximal air consumption of one nozzle approximately equaled 200 l/min, thus measurements were carried out up to this value. Figure 23 and Figure 25 display the weld depth as a function of the air speed and approximate flow rate at 4 kW and 6 kW. The flow rates are given in brackets.

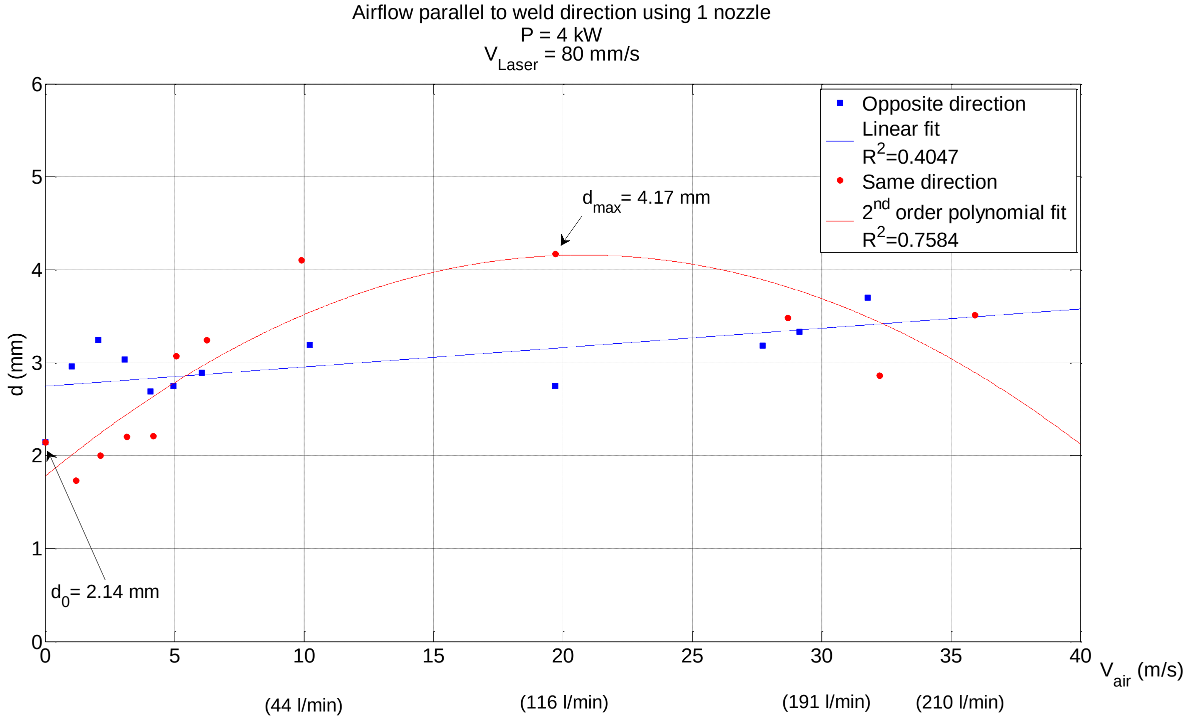

Figure 23 Weld depth vs. airspeed at 4 kW while airflow was parallel to weld direction.

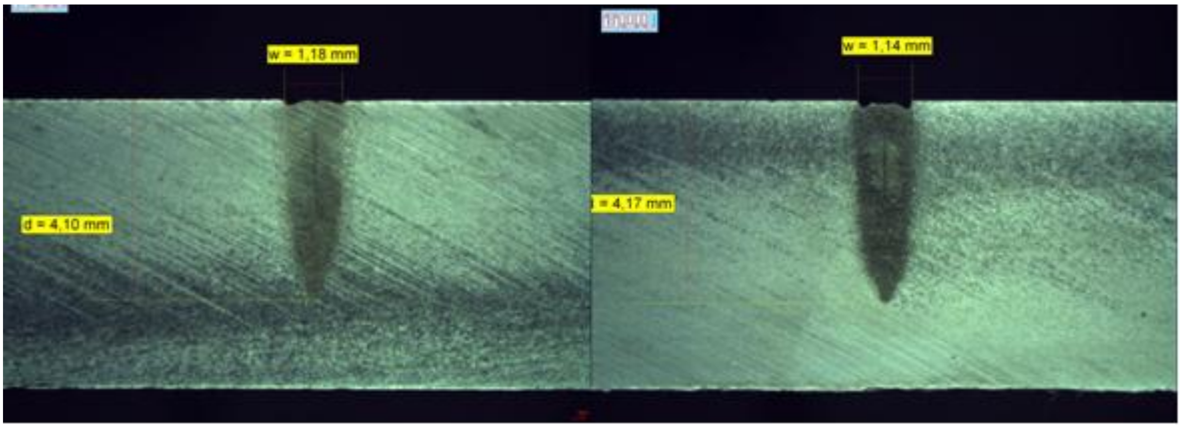

Figure 24 The cross sections of welds obtained at $V_{air} \approx 10$ m/s and $V_{air} \approx 20$ m/s.

The cross sections of Figure 24 belong to the same direction case of Figure 23. Above figure displays the welds with approximately the same depth. The quality of the weld seems to be good.

Instead of drawing lines from one data point to the other, linear and second order polynomial fits are applied to represent the data in the d vs. V_{air} plots. With these fits more insight is given regarding the trend the weld depth follows as the air speed increases.
The R^2 value of each fit is given in the legend, and indicates how successful the fit is in explaining the variation of the data points [9]. If this value is close to one, the fit is a good model for representation of the data points.

At first sight, the discrete data points of the same direction case in Figure 23 appear to increase, reach a maximum, and then start to decrease. A 2nd order polynomial was chosen as a fit, and a R^2 value of 0.758 was obtained. Thus the 2nd order fit is an appropriate choice.

Air blown in the same direction as the weld direction at 4 kW led to the deepest weld i.e. d_{max}= 4.17 mm at approximately 20 m/s and 116 l/min while the weld depth at zero air velocity equaled 2.14 mm. This is a significant increase of 2.03 mm.
On the other hand, if air was blown in opposite direction, a high air velocity greater than 40 m/s and flow rate greater than 210 l/min would be needed to obtain a deep weld of 4 mm.
So, the same direction case gave the best result since the deepest weld was obtained at lower air consumption.
As suggested in section 1.1, high air speeds will decrease the weld quality by blowing the molten material way. Further research is needed to give a definite conclusion concerning this matter.

In Figure 25 the data of the same direction case at 6 kW is split up into two parts because at low air speeds the depth displays an increasing trend while the depth at high air speeds seems to be relatively constant. The first data set lies between 0-10 m/s and the second data set lies between 20-35 m/s.

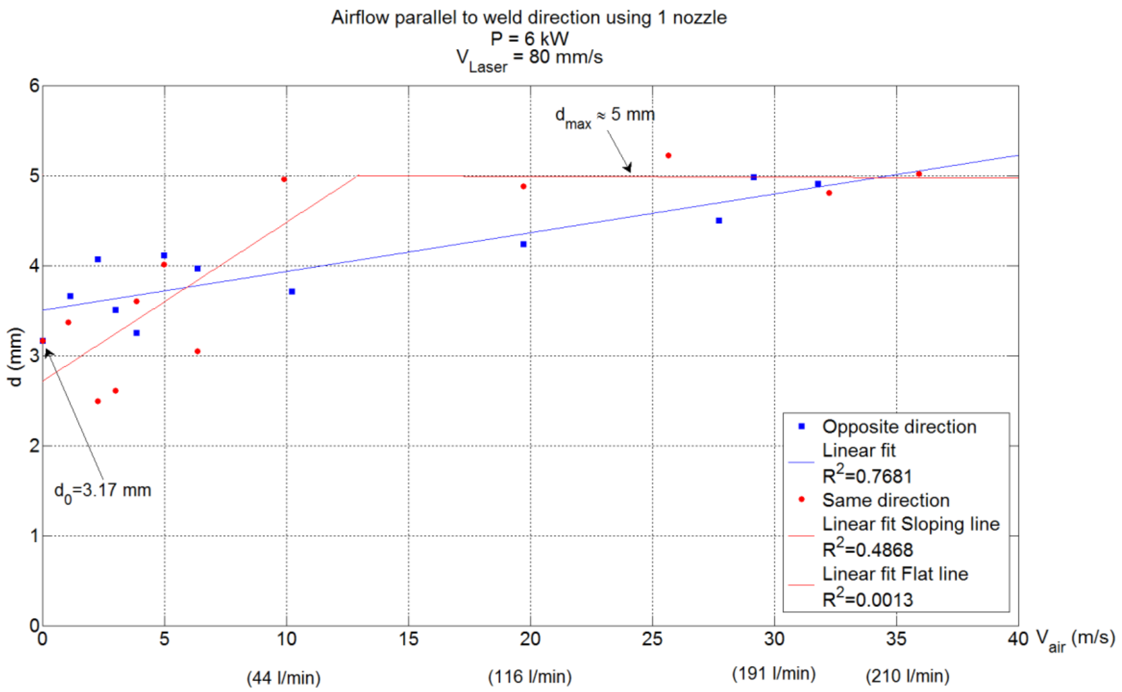

Figure 25 Weld depth vs. airspeed at 6 kW while airflow was parallel to weld direction.

Air blown in the same direction at 6 kW led to the deepest welds of approximately 5 mm while the depth at zero air velocity equaled 3.17 mm. This is an increase of 1.83 mm.
Interesting is that this maximum depth is reached at $V_{air}\approx$ 13 m/s and 44 l/min, yet stays relatively constant for higher velocities.
For the opposite direction case, the weld depth equals 5 mm at approximately V_{air}= 34 m/s and 210 l/min. So, the same direction case gave the best result since the weld was deepest at lower air consumption.
If the discrete measurements are observed at low airspeeds between 0-6 m/s, air blown in opposite direction gave deeper welds compared to the same direction case.

Both same direction cases at 4 and 6 kW gave increased depths of around 2 mm. The cross section of the welds at different air speeds is given in Figure 26. These cross sections belong to the same direction case. In Appendix 3 these cross sections are displayed with accompanying depths.

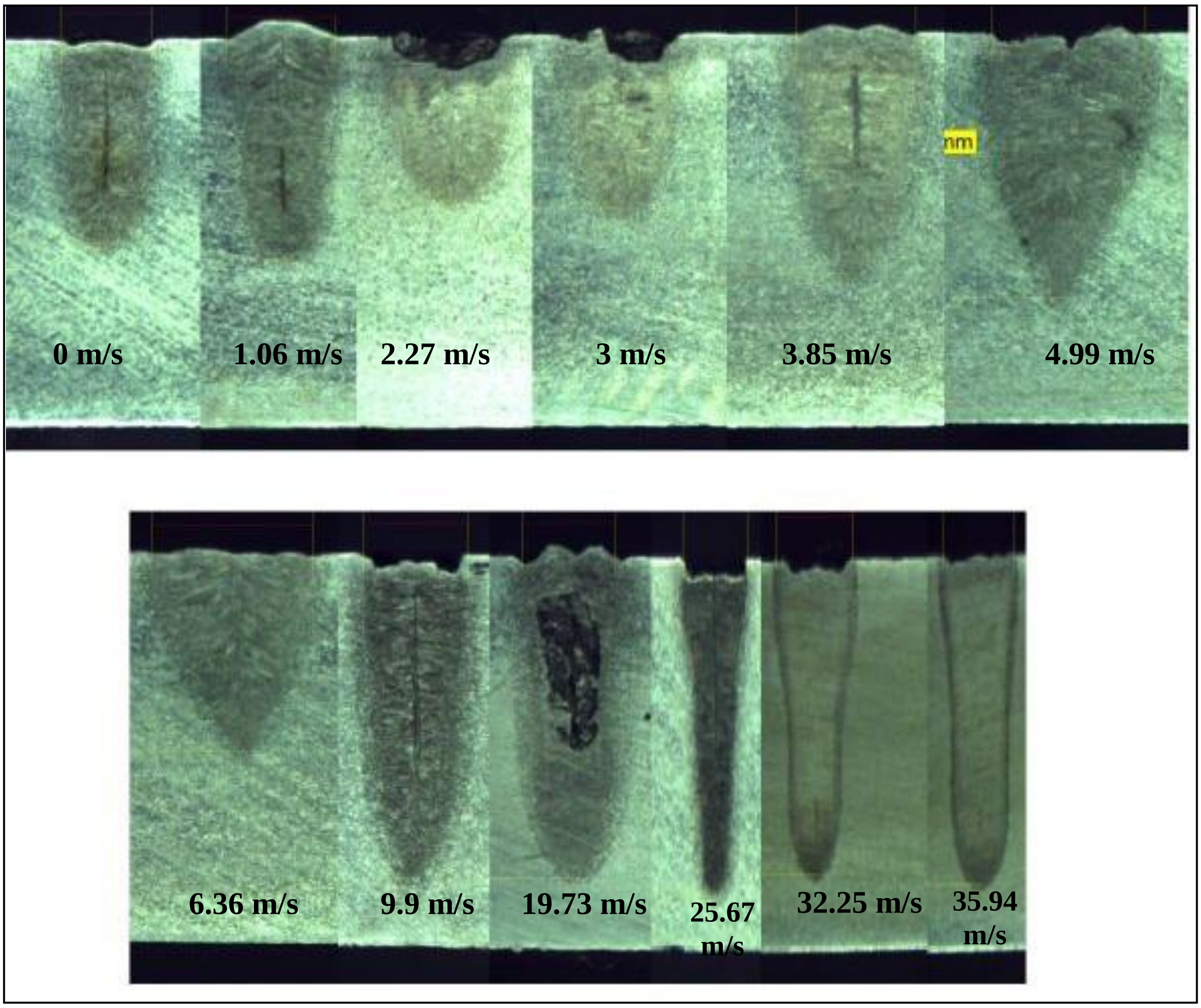

Figure 26 Cross sections at increasing air velocity at 6 kW. Air was blown in same direction as the weld direction.

4.3 Application of an array of nozzles

Previous results led to the following conclusions:

- Air should be blown parallel to the weld because air that is blown perpendicular gives the shallowest depth.
- When using one nozzle, the nozzle height should lie at 10 mm; if an array of nozzles is used, they should all lie above 10 mm.

The objective of applying six nozzles was to obtain an air profile that was as flat as possible between the optical head and test piece surface. This was achieved by placing the nozzles 200 mm away from the weld and increasing the flow rate. Since six nozzles were used, the maximum air consumption increased considerably in comparison with one nozzle i.e. the maximum flow rate equaled approximately 250 l/min at V_{air}= 6 m/s. During the measurements, the flow rate was varied between 150-250 l/min, with intervals of 25 l/min. At flow rates below 150 l/min, the air profile contained regions with very low (nearly zero) velocity.

Figure 27 and Figure 29 display the weld depth as a function of air velocity and flow rate.

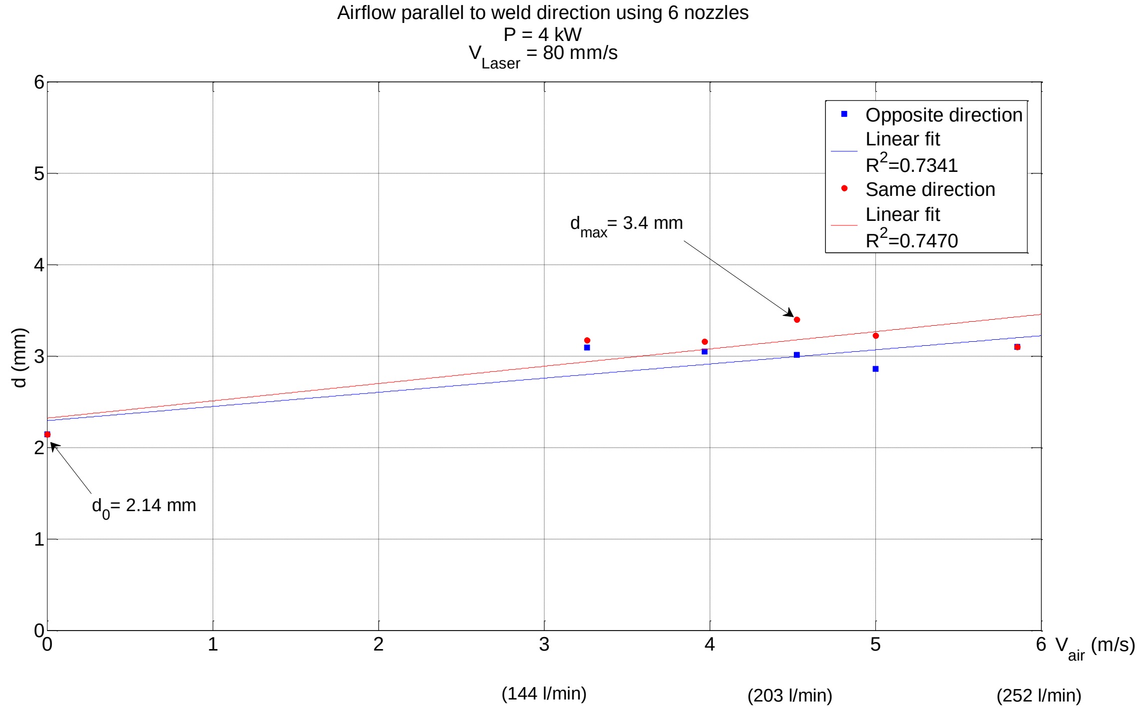

Figure 27 Weld depth vs. airspeed at 4 kW while airflow was parallel to weld direction; six nozzles were used. .

In Figure 27 the linear fits show that the deepest welds were obtained when air blew in the same direction as the weld direction. The deepest weld equaled 3.4 mm, while d_0 was 2.14 mm; this is an increase of 1.26 mm. Also, the results in both directions do not differ much.
Figure 28 displays the cross sections of the welds for the same direction case. In Appendix 3 these cross sections are displayed with accompanying depths.

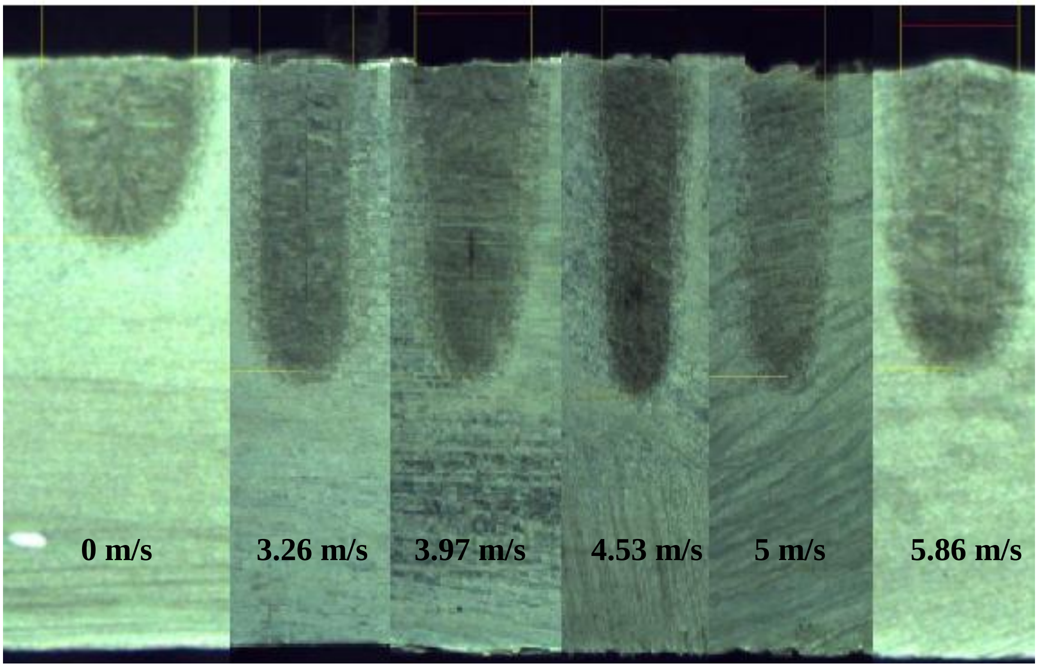

Figure 28 Cross sections at increasing air velocity at 4 kW. Air was blown in same direction as the weld direction.

When welding at 6 kW (Figure 29), the linear fits for both the same direction as the opposite direction case do not differ much. If discrete data points are observed, the weld depths are actually equal i.e. at 4 and 5 m/s both cases give the same weld depth of 4.33 mm. So, for 6 kW no specific blowing direction can be suggested. The weld depth increased with 1.16 mm when compared to the depth at zero velocity.

With six nozzles, there was less scatter in the d vs. V_{air} plot between 0-6 m/s than with one nozzle. If the discrete measurements in Figure 27 and Figure 29 are observed closely, there is actually a constant trend between 3 and 6 m/s.
The weld depths in Figure 27 and Figure 29 were lower than in the one nozzle situation because the air velocity above the weld was too low to blow away the low refractive index zone.

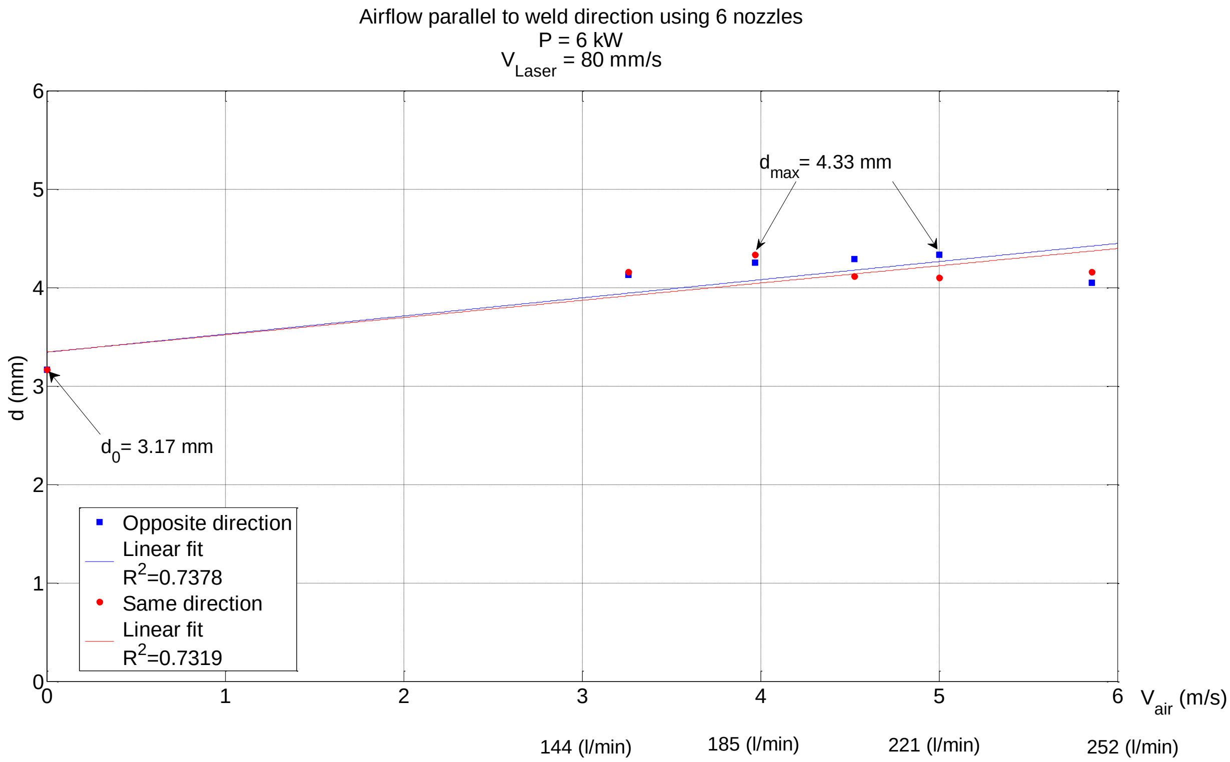

Figure 29 Weld depth vs. airspeed at 6 kW while airflow was parallel to weld direction; six nozzles were used.

Unfortunately, the air pressure in the test cell was limited and the further course of the d vs. V_{air} plot could not be obtained. The maximum air velocity equaled around 6 m/s while the air consumption equaled 252 l/min. As seen in Figure 23 and Figure 25, interesting developments start to take place above 10 m/s. Research at higher air velocities with six nozzles is thus strongly advised, and no optimal air consumption can be specified for the six nozzle case.

4.4 Longitudinal section of welds

The weld depth in this report is continually measured in the cross (transverse) section, but additional insight is gained when viewing the longitudinal section of the weld. Particularly, the scattered weld depths in Figure 23 and Figure 25 (between 0-6 m/s) was investigated by viewing the longitudinal section.
Figure 30 and Figure 31 each display two welds above each other i.e. the upper weld was obtained at zero air velocity and the lower weld was obtained by blowing air at approximately $V_{air} \approx 31.8$ m/s and 190 l/min with one nozzle at a height of 10 mm.

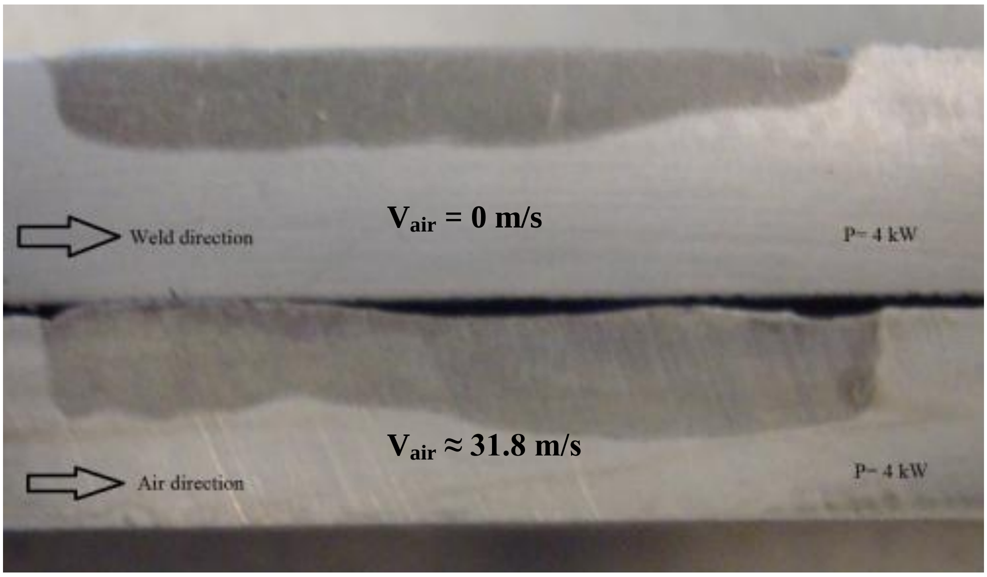

Figure 30 Longitudinal section of welds with length of 20 mm and obtained at 4 kW. Upper weld is obtained at V_{air}=0 m/s and the lower weld is obtained at $V_{air} \approx 31.8$ m/s and q = 190 l/min with one nozzle. (Both welds are displayed on the same scale)

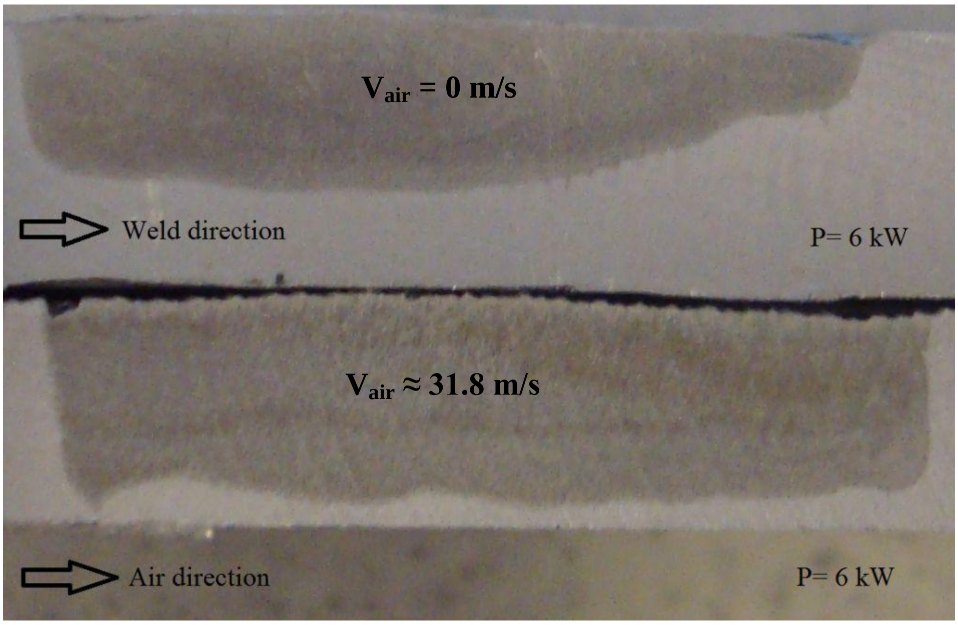

Figure 31 Longitudinal section of welds with length of 20 mm and obtained at 6 kW. Upper weld was obtained at V_{air}=0 m/s and the lower weld was obtained at $V_{air} \approx 31.8$ m/s and q = 190 l/min. (Both welds are displayed on the same scale)

The fluctuating weld depth in above figures is thought to be the cause of the scattered measurements in Figure 23 and Figure 25.

The welds at zero air velocity are relatively constant at first, and then start to decrease in depth. This is the case for both 4 and 6 kW. Defocusing and refraction of the Laser beam by heated air is assumed to be the cause. At the start of the weld surrounding air is not heated much, so there is little effect from this heated zone. But as the weld progresses to the right, the air above the weld is heated enough to defocus and refract the Laser beam considerably and affect the weld depth.

In each of the below figures the maximal and minimal depth belonging to the longitudinal sections are displayed.

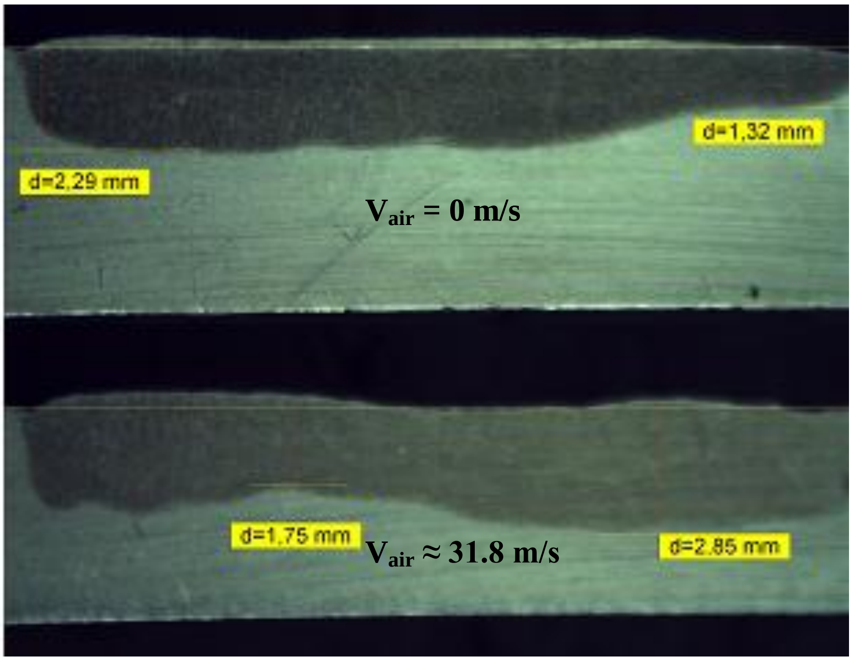

Figure 32 Weld depths at 4 kW belonging to Figure 30.

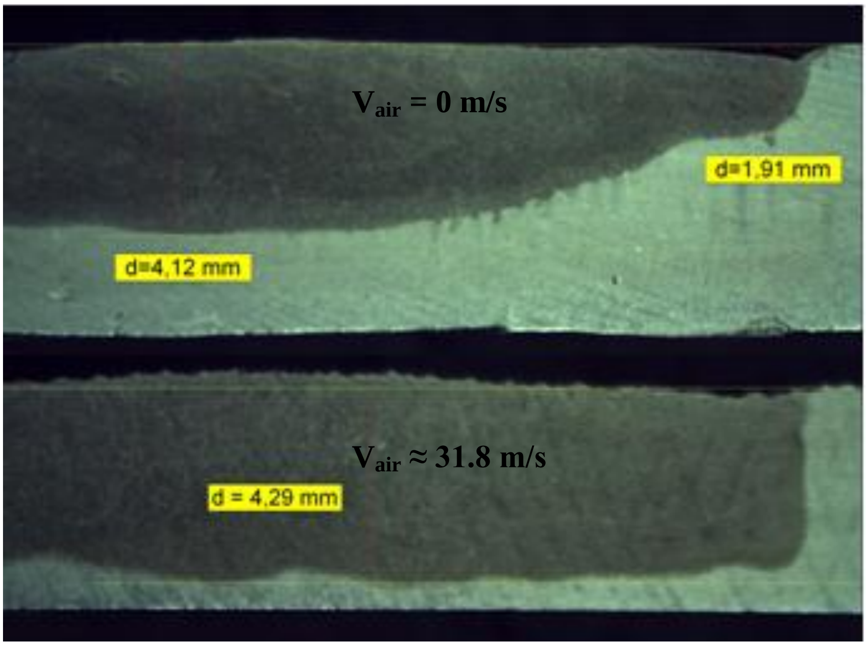

Figure 33 Weld depths at 6 kW belonging Figure 31.

At 4kW the weld depth decreases a little when air is blown, but the depth increases as the weld progressed to the right.
At 6 kW the weld depth increased over the entire length when air was blown. Especially at the end of the weld, the increase in depth is significant when compared to the zero air velocity case.
This effect was also proven in literature [2, 3], as is displayed in Figure 3 and Figure 4. Future research with longer welds and longitudinal sections should give more insight into the depth increase while blowing air.

The experimental setup, as displayed in Figure 9 and Figure 14, had to be dismantled and constructed again quite frequently because of usage of the test cell by others.
This caused some daily variations in the height of the nozzles and loosening of the fitting of the pressure tubes. These defects were corrected as soon as they were discovered.

5 Conclusions and recommendations

5.1 Conclusions

After literature research, the following conclusions were drawn:

- The low refractive index zone is the leading cause for the decrease in weld depth during fiber Laser welding. This zone defocuses and refracts the fiber Laser beam.

- The atmosphere above the weld pool must be kept fresh to obtain deeper welds. Shielding gasses such as Helium are a good choice to blow away this index zone, but this report proves that application of cheaper gasses such as air is sufficient.

- The low refractive index zone is a localized zone, so it is not required to blow air throughout the whole cell.

- The size of the low refractive index zone changes strongly as time passes. So, a fixed rule for the optimal amount of air needed to obtain deeper welds, is not easily determined.

In this report an experimental setup was designed and built to find the optimal air conditions. After analyzing the experimental results, the following conclusions were drawn:

- At low power levels, air does not improve the weld depth, as is displayed in Figure 18. This is because the atmosphere above the weld pool is not heated significantly at low power level, thus the application of blowing air does not improve the weld depth.
- From 4 kW upwards, blowing air does influence the weld depth.
- The results in section 4.1 indicate that the deepest welds were obtained by blowing at a height of 10 mm above the test piece surface.
- The application of air not only influences the weld depth, but also the appearance of the weld, as is displayed in Figure 19.
- The plots in section 4.2 show that the weld depth increased 2.03 mm at 4 kW and 1.8 mm at 6 kW while using a single nozzle.
- If the fitted curves in section 4.2 are analyzed, the optimal amount of air needed for the deepest weld at 4 kW was 116 l/min at 20 m/s. While at 6 kW, the optimal amount of air was just above 44 l/min at 13 m/s.
  If the discrete measurements are studied at 4 kW (Figure 23), the optimal amount of air is 44 l/min at 10 m/s.
- With one nozzle, the air direction should be in the same direction as the weld.

- The results from section 4.3 show that if six nozzles were used, the deepest welds were lower than with one nozzle because the air velocity was very low i.e. between 0-6 m/s. With six nozzles, the weld depth increased 1.26 mm at 4 kW and 1.16 mm at 6 kW when compared to the depth at zero velocity.

- With six nozzles, there was less scatter in the d vs. V_{air} plot between 0-6 m/s than with one nozzle. Thus, these results are more reliable. If the discrete measurements in Figure 27 and Figure 29 are observed closely, there is actually a constant trend between 3-6 m/s.

- Also, no specific blowing direction could be determined when using six nozzles, since the fitted curves nearly overlapped at 4 and 6 kW.

- It is premature to accept these conclusions, concerning the array of nozzles, as a final result since measurements were only carried out at low velocities.

5.2 Recommendations

Recommendations for further research

- The influence of varying the welding speed while blowing air should be studied.
- Longitudinal section of welds longer than 20 mm will give more insight into the influence air has on the weld depth.
- By measuring the temperature of the atmosphere above the weld, the refractive index can be approximated, and a closed loop controller could be designed to control the air velocity as a function of the refractive index in order to obtain a desired weld depth.

Recommendations for AWL-Techniek

- The application of air while welding with a fiber Laser has a significant influence on the welding depth. Therefore, AWL should continue to use an airflow in Laser welding.

- A single nozzle works best at high air velocities above 10m/s and between 20-25 m/s the deepest welds were found (Figure 23 and Figure 25).

Unfortunately, the air pressure in the test cell was limited, and no measurements were carried out at higher velocities with six nozzles. If the array of nozzles was positioned closer to the welds, the air velocity increased. But, in this situation, the air profile was discontinuous i.e. the air profile contained regions with very low (nearly zero) velocity.
If future measurements are done at higher air velocities, the air consumption will be very high i.e. above 250 l/min.

- Because of production applications, it is recommended to generate an air profile with a fan or airknife and not with an array of nozzles. The form of the air profile is hard to control with these devices, but both give a continuous air profile, and are not fed with pressurized air.

References

[1] Mark Faerber, Joe Berkmanns, and Wolfgang Danzer. Welding with air shielding. In *Industrial Laser Solutions for Manufacturing.*

[2] Shinpei Oiwa, Yosuke Kawahito, and Seiji Katayama. Plume behavior and refractive index distribution during Laser welding. In *Proceedings of LAMP2009 - the 5th International Congress on Laser Advanced Materials Processing*.

[3] Shinpei Oiwa, Yosuke Kawahito, and Seiji Katayama. Optical properties of Laser-induced plume during high power Laser welding. In *ICALEO 2009*, *paper #708*.

[4] P.Yu. Shcheglov, S.A. Uspenskiy, A.V. Gumenyuk, V.N. Petrovskiy, M. Rethmeier, and V.M. Yermachenko. Plume attenuation of Laser radiation during high power fiber Laser welding. In *Laser Physics Letters 8, No. 6, pages 475–480, 2011*.

[5] Interferometry. http://en.wikipedia.org/wiki/Interferometry

[6] W.W. Duley. Laser welding. John Wiley & sons, Inc., Canada, 1999.

[7] Scattering. http://en.wikipedia.org/wiki/Scattering

[8] Fringe pattern. http://en.wikipedia.org/wiki/Fringe_shift

[9] MatLab Product Help, MathWorks, Inc.

Appendices

Appendix 1 Work plan

Week	Activity
35	Settling into the company Subject formulation Study company literature concerning robots and laser welding
36	Participate in company course: working in Lasercel (duration of two days) Start literature search and study
37	Literature search and study
38	Design and build experimental set up
39	Measure and optimize experiment
40	Measure and optimize experiment
41	Measure and optimize experiment
42	Measure and optimize experiment Compare experiment results with literature
43	Measure and optimize experiment
44	Measure and optimize experiment
45	Measure and optimize experiment
46	Measure and optimize experiment
47	Write report
48	Company presentation

Appendix 2 Measurement devices

Below table displays the used measurement devices.

Device	Type
Control valve	Festo GR-Q5-0
Flow Sensor	Festo SFAM-62-5000L-TG12-25V-M12
Pressure Sensor	Festo SPAB-P10R-G18-2P-M8
Air Nozzle	Silvent 961
Fiber Laser	IPG YLS 6000
Laser Power Meter	Primes PocketMonitor 70icu
Microscope	Novex RZT SF 65.560
Anemometer	Höntzsch HTA

Table 3 Measurement devices.

One-way flow control valves GR/GRA, in-line installation

FESTO

Technical data – Female thread, metal

One-way flow control function

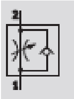

Flow rate
29.5 ... 3,300 l/min

Temperature range
−20 ... +75 °C

Operating pressure
0.1 ... 15 bar

General technical data							
Valve function	One-way flow control function						
Pneumatic connection 2	M3	M5	G⅛	G¼	G⅜	G½	G¾
Pneumatic connection 1	M3	M5	G⅛	G¼	G⅜	G½	G¾
Adjustment component	Knurled screw						
Type of mounting	Via through-hole						
	Front panel mounting						
Mounting position	Any						

Note: This product conforms with the ISO 1179-1 standard and the ISO 228-1 standard.

Operating and environmental conditions							
Pneumatic connection 2	M3	M5	G⅛	G¼	G⅜	G½	G¾
Operating pressure [bar]	0.3 ... 8	0.5 ... 10		0.1 ... 10			0.3 ... 15
Operating medium	Filtered compressed air, lubricated or unlubricated						
	Grade of filtration 5 µm	Grade of filtration 40 µm		–			
Ambient temperature [°C]	−10 ... +60	−20 ... +60		−20 ... +75			−10 ... +60
Temperature of medium [°C]	−10 ... +60	−20 ... +60		−20 ... +75			−10 ... +60
Storage temperature [°C]	−10 ... +40	−20 ... +60		−20 ... +75			−10 ... +60

Standard nominal flow rate qnN at 6 → 5 bar as a function of turns of the adjusting screw n

GR-M3

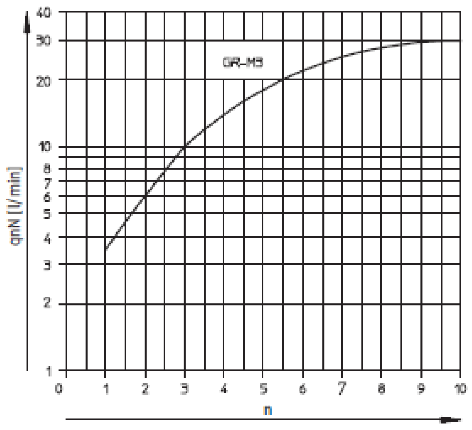

GR-M5-B, GR-⅛-B, GRA-¼-B

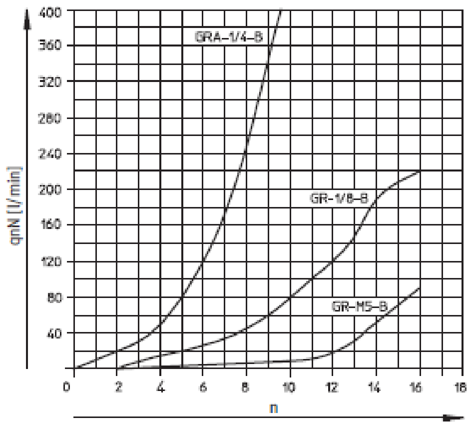

Appendix 2.2 Flow Sensor

Flow sensors SFAM

FESTO

Technical data

Input signal/measuring element							
Type		SFAM-62			SFAM-90		
Flow measuring range		-1000	-3000	-5000	-5000	-10000	-15000
Measured variable		Flow rate, consumption					
Direction of flow	-L	Unidirectional P1 ⟶ P2					
	-R	Unidirectional P2 ⟵ P1					
Measuring principle		Thermal					
Flow measuring range	[l/min]	10 ... 1,000	30 ... 3,000	50 ... 5,000	50 ... 5,000	100 ... 10,000	150 ... 15,000
Operating pressure	[bar]	0 ... 16					
Nominal pressure	[bar]	6					
Operating medium		Air quality class 5:4:3 to DIN ISO 8573-1					
		Nitrogen					
Temperature of medium	[°C]	0 ... +50					
Ambient temperature	[°C]	0 ... +50					
Nominal temperature	[°C]	23					

Output, general[1), 2)]		
Accuracy of zero point in ±%FS	[%FS]	0.3
Accuracy of margin in ±%FS	[%FS]	3
Repetition accuracy of zero point in ±%FS	[%FS]	0.2
Repetition accuracy of margin in ±%FS	[%FS]	0.8
Temperature coefficient of margin in ±%FS/K	[%FS/K]	Typically 0.1
Pressure dependence of margin in ±%FS/bar	[%FS/bar]	0.5

1) Accuracy with nominal conditions (6 bar, 23 °C and horizontal installation position)
2) %FS = % of the measuring range final value (full scale)

Switching output		
Switching output		2x PNP or 2x NPN, adjustable
Switching function		Window comparator or threshold value comparator, adjustable
Switching element function		N/C or N/O contact, adjustable
Switch-on time		Adjustable (factory setting: approx. 60 ms)
Switch-off time		Adjustable (factory setting: approx. 60 ms)
Max. output current	[mA]	100
Voltage drop	[V]	Max. 1.5
Inductive protective circuit		Adapted to MZ, MY, ME coils

Analogue output							
Type		SFAM-62			SFAM-90		
Flow measuring range		-1000	-3000	-5000	-5000	-10000	-15000
Characteristic curve for flow rate	[l/min]	0 ... 1,000	0 ... 3,000	0 ... 5,000	0 ... 5,000	0 ... 10,000	0 ... 15,000
Output characteristic curve for current	[mA]	4 ... 20					
Output characteristic curve for voltage	[V]	0 ... 10					
Rise time	[ms]	Possible settings: 15, 30, 60 (factory setting), 125, 250, 500, 999					
Max. load resistance at current output	[ohms]	500					
Min. load resistance at voltage output	[kohms]	10					

Output, additional data	
Protection against short circuit	Yes
Protection against overloading	Yes

Appendix 2.3 Pressure Sensor

New variants

Pressure sensors SPAB, with display

FESTO

Technical data

Function

E.g. switching output 2x PNP

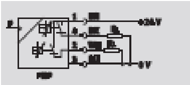

E.g. switching output NPN, analogue output

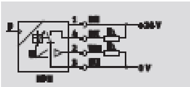

Voltage

12 ... 24 V DC

Pressure

−1 ... +10 bar

Temperature range

−10 ... +50 °C

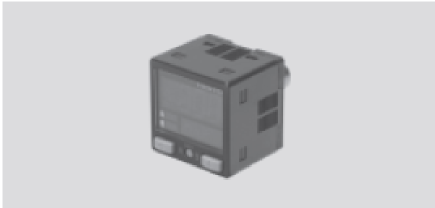

General technical data			
SPAB		-B2	-P10
General information			
Certification		cULus listed (OL)	
		C-Tick	
CE mark (see declaration of conformity)		To EU EMC Directive[1]	
Note on materials		Contains PWIS (paint wetting impairment substances)	
		RoHS-compliant	
Input signal/measuring element			
Measured variable		Relative pressure	
Measurement method		Piezoresistive pressure sensor with display	
Pressure measuring range	[bar]	−1 ... +1	0 ... 10
Overload capacity	[bar]	5	15
Operating medium		Filtered, unlubricated compressed air, grade of filtration 40 µm	
Ambient temperature	[°C]	−10 ... +50	

1) For information about the applicability of the component see the manufacturer's EC declaration of conformity at: www.festo.com → Support → User documentation.
If the component is subject to restrictions on usage in residential, office or commercial environments or small businesses, further measures to reduce the emitted interference may be necessary.

Electrical data									
SPAB		-B2				-P10			
Electrical output		2P	2N	PB	NB	2P	2N	PB	NB
Switching output[1]									
Switching output		2x PNP	2x NPN	PNP	NPN	2x PNP	2x NPN	PNP	NPN
Switching function		Freely programmable							
Switching element function		Switchable							
Accuracy of FS display	[%]	1				2			
Reproducibility of switching value	[%]	0.1				0.2			
Max. output current	[mA]	100							
Analogue output[1]									
Analogue output	[V]	–		1 ... 5		–		1 ... 5	
Accuracy of analogue output zero point ±FS	[%]	–		5		–		5	
Accuracy of analogue output margin ±FS	[%]	–		5		–		5	
Reproducibility of analogue value	[%]	–		0.2		–		0.2	
Output, additional data									
Protection against short circuit		Yes							

1) % FS = % of the measuring range final value (full scale)

Appendix 2.4 Air Nozzle

Silvent 961

SILVENT 961: a small, angled flat nozzle that generates a broad but thin air cone. Small mounting dimensions make it especially suitable for machine designs where space limitations are a problem. In many cases mounting is facilitated by the fact that the blowing angle is perpendicular to the plane of the threads. Can also be mounted in a manifold array, creating compact, quiet and efficient air knives. Made of zinc. The outlet orifices are protected against external forces by fins. SILVENT 961 fulfills the requirements the EU Machine Directive stipulates regarding airborne noise from machines and fully meets OSHA safety regulations. Patented.

4 mm (5/32")

Noise reduction	60%
Air/cost savings	33%

** When replacing open pipe of this diameter*

Technical data Accessories Compare Files

Specifications

	SI units	US units
Blowing force	3.3 N	11.6 oz
Air consumption	19.5 Nm³/h	11.5 scfm
Sound level	81.5 dB(A)	
Air pattern	Flat	
Connection	1/8" BSP	1/8"-27 NPT
Connection type	Male	
Dimensions	23.9x23.5x13.4 mm	0.94x0.93x0.53 inch
Material (nozzle)	Zinc	
Weight	0.018 kg	0.040 lbs
Max temp	70 °C	158 °F
Max operating pressure	1.0 MPa	143.0 psi

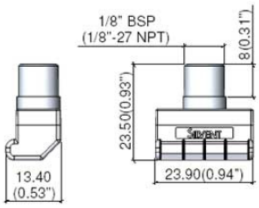

Benefits

Replace open pipe	4 mm	5/32 inch
Noise reduction	13 dB(A)	60 %
Air/cost savings	10 Nm³/h	5.9 scfm
Fulfill OSHA standards	Yes	
Meet the EU Machine directives	Yes	

Product search
>>

ABOUT SILVENT PRODUCTS APPLICATIONS TECHNOLOGY COMPETENCES

Blowing force (N)	1.3	2.6	3.9	5.1	6.6
Air consumption (Nm³/h)	9.0	15.5	22.7	29.6	36.5
Sound level (dB(A))	71.1	78.1	82.8	85.5	87.6
US units (psi)	**40**	**60**	**80**	**100**	**120**
Blowing force (oz)	6.4	9.7	12.7	15.7	19.4
Air consumption (scfm)	6.9	9.4	12.4	15.2	18.1
Sound level (dB(A))	73.7	78.4	82.2	84.0	85.9

Air cone patterns and velocity distribution

SI units (mm)	**50**	**100**	**200**	**300**	**400**	**500**
Air pattern (width)	63	82	120	160	200	240
Air pattern (height)	30	50	90	130	170	210
Velocity (m/s)	122	100	57	40	36	33
US units (inch)	**2**	**4**	**8**	**12**	**16**	**20**
Air pattern (width)	2.48	3.23	4.72	6.30	7.87	9.45
Air pattern (height)	1.18	1.97	3.54	5.12	6.69	8.27
Velocity (ft/s)	400	328	187	131	118	108

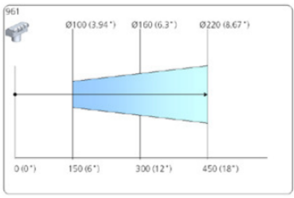

PHOTONICS

YLS Series

Product Designation*	YLS-XXXX	YLS-XXXX
Description	Compact kW Fiber Laser System	kW Class Fiber Laser System
Standard Features	Randomly polarized, 1070-1080 nm emission wavelength, ytterbium doped, red aiming diode	Randomly polarized, 1070-1080 nm emission wavelength, ytterbium doped, red aiming diode
Available Operating Modes	CW, QCW, SM	CW, QCW, SM
Available Output Power	500 Watts - 2 kW	500 Watts - 50 kW
Feed Fiber Diameter*	Available in single-mode, 50, 100, 200 or 300 µm diameter	Available in single-mode, 50, 100, 200 or 300 µm diameter, options dependant upon power
Wall-plug Efficiency	>30%	>30%
Output Termination Options	HLC-8 (QBH type) & LCA (QD type)	HLC-8 (QBH type), HLC-16, & LCA (QD type)
Ancillary Options	External coupler, External 1x2, 1x4 or 1x6 beam switch or External 50:50 beam splitter	Internal coupler, beam shutter, 1x2, 1x3 or 1x4 beam switch or 50:50 beam splitter External 1x6 beam switch
Air Conditioner	Standard	Standard
Interface	Standard: LaserNet, Digital I/O, Analog Control Additional Options: DeviceNet, Profibus or Ethernet	Standard: LaserNet, Digital I/O, Analog Control Additional Options: DeviceNet, Profibus or Ethernet
Cabinet Style/ Dimensions	12U Standalone NEMA 12 Enclosure (HxWxD, mm) 558x790x815	1-4 kW: 25U Standalone NEMA 12 Enclosure (HxWxD, mm) 1106x856x806 5-10 kW: 31U Standalone NEMA 12 Enclosure (HxWxD, mm) 1400x856x806
Reserve Module	Available option for <2 kW, Standard on 2 kW	Available option for <2 kW, Standard on 2 kW+
Upgradeable	Yes, maximum 2 kW	Yes, 25U cabinet max 4 kW, 31U max 10 kW

SYSTEM NOMENCLATURE

When ordering an IPG Fiber Laser System, if any optics are internal to the system or the chiller is affixed, the part number of the system will change accordingly. Below is a small sampling of possible configurations and what the resulting part number would be. Note that the numerics are based out power output. Information on our optics is available on the following page.

Cabinet	Power	Direct Feed Fiber	Internal Coupler	Internal Beam Shutter	Internal 1x2 Switch	Internal 1x3 Switch	Internal 1x4 Switch	Internal 1x2 Beam Shearer	Affixed Chiller no Optics	Affixed Chiller with Optics
6U Rack Mount	≥1,000 Watts	YLR-1000	NA	NA	NA	NA	NA	NA	YLR-1000-TR	NA
12U NEMA 12 Enclosure	≥2,000 Watts	YLS-2000	NA	NA	NA	NA	NA	NA	YLS-2000-TR	NA
25U NEMA 12 Enclosure	≥4,000 Watts	YLS-4000	YLS-4000-CT	YLS-4000-S1T	YLS-4000-S2T	YLS-4000-S3T	YLS-4000-S4T	YLS-4000-SS2T	YLS-4000-TR	YLS-4000-XX-TR*
31U NEMA 12 Enclosure	4,000-10,000 Watts	YLS-10000	YLS-10000-C	YLS-10000-S1	YLS-10000-S2	YLS-10000-S3	YLS-10000-S4	YLS-10000-SS2	YLS-6000-TR**	YLS-6000-XX-TR*

PocketMonitor

Technical Data:

Power range:	1 W to12 kW (depending on size of the absorber)
Resolution:	1 W (PMT 120 icu) - 0.01 W (PMT 002p)
Dynamics:	20 bit A/D converter
Exposure time:	10 or 20 seconds
Life span (battery):	extremely long, approximately 10,000 measurements
Display:	4½ digit LCD, integrated in a robust aluminium housing (IP65)

In measuring position (open), the length of the device is 279 mm. The diameter of the absorber is 79 mm (Model 70icu).

Accuracy of the PocketMonitor is ± 4 % of the measured value in the range of 10 % to 100 % of the maximum value.
Reproducibility: 2 %; in the case of careful dis-section 1%

Power density often can be as important for the choice of a PocketMonitor model as the maximum laser power. Especially the PMT 70icu and the PMT 120icu have an outstanding capacity for high power densities. With these two types, even measurements at 5 kW/cm² with 5 kW optical power are possible.

Options

The PocketMonitor ist not only available with different absorber sizes, even separated ab-sorbers are possible.

Additionally, an optional current loop interface and an OEM version for mechanical integration is available.

A transportation box for safe shipment and storage has been conceived.

The option for calibration completes the choice. Constant recalibrating is recommended.

All options could be combined with all instruments. This leads to a most complete and flexible measurement device.

We are glad to assist you in your choice of the right PocketMonitor for your application.

Transportation box for the PocketMonitor

PocketMonitor Model 05 with separated absorber

PocketMonitor 70icu with separated absorber and handle

Microscope: Novex trinocular zoom sterio microscope RZT SF 65.560
CMEX DC 5000
Colour USB2 Camera
Serial# 5219
euromex.com

The E-series and Z-series

Stereo microscopes are often used in science and industry for research, inspection, manufacturing or modification of extremely small objects.

Due to its high contrast and wide field of view, stereo microscopes are perfectly suitable for such. The E- and Z-series microscopes are used in a wide variety of applications for medical doctors, biologists, tooth technicians and renovators.
In the electronics, fine mechanical, galvanic, graphical and food industry these high quality microscopes series are used for research and quality control due to their brilliant optical performance.

Configuration: EE.1552 and ST.1740

Stereo heads E-series 45° tube, with 2 pair objectives in revolving nosepiece

EE.1521 - binocular	EE.1522 - binocular EE.1552 - trinocular	EE.1523 - binocular EE.1553 - trinocular	EE.1524 - binocular EE.1554 - trinocular
Objectives 0.5x and 1x Magnification 5x and 10x Field number 46 and 23 mm Free working distance 200 mm Specifically for stands ST.1715, ST.1720, ST.1770, ST.1780, ST.1785	Objectives 1x and 2x Magnification 10x and 20x Field number 23 and 11.5 mm Free working distance 110 mm	Objectives 1x and 3x Magnification 10x and 30x Field number 23 and 7.7 mm Free working distance 80 mm	Objectives 2x and 4x Magnification 20x and 40x Field number 11.5 mm and 5.7 mm Free working distance 63 mm

Stereo heads Z-series with zoom objective

ZE.1624 - binocular* ZE.1654 - trinocular*	ZE.1670 - binocular ZE.1671 - trinocular	ZE.1626 - binocular	ZE.1629 - binocular	ZE.1657 - trinocular	ZE.1659 - trinocular
Tube 45° Zoom objective 0.7x - 4.5x Magnification 7x - 45x Field number 32 - 5.1 mm Free working distance 93 mm	Tube 45° Zoom objective 1x - 7x Magnification 10x - 70x Field number 23 - 3.29 mm Free working distance 104 mm ZE.1671: when using photo tube the image remains visible in both eyepieces	Similar to ZE.1624 but with 60° tube, suitable to mount on instruments or machines Free working distance 93 mm	Similar to ZE.1624 but with 90° tube, suitable to mount on instruments or machines Free working distance 110 mm	Similar to ZE.1654 but **when using photo tube the image remains visible in both eyepieces!** Free working distance 104 mm	Similar to ZE.1657 but with Zoom objective 0.4x - 2.5x Magnification 4x - 25x Free working distance 185 mm **With opening for flexible light conductor for semi coaxial illumination**

* For click-stop versions, add suffix '-D' to article number

Appendix 2.8 Anemometer

Operating Instructions HTA Version 1.1

A handy and easy-to-use anemometer for measuring standard flow velocity, standard volume flow and temperature of air/gases (standard conditions: +21 °C, 1014 hPa).

Höntzsch thermal flow sensors with thin-film sensor element can be connected to the HTA display unit for combined measurement of flow and temperature: Probes TA10 ... ZG1b and measuring tubes TA-Di ... ZG2b

HTA Page 1 of 7	U238 6/2001

höntzsch
flow measuring technology

Höntzsch GmbH • P.O.Box 1324 • 71303 Waiblingen

CaTeC b.v.
Turfschipper 114
2292 Wateringen
Niederlande

Delivery Note No.: RL09-0231
Delivery date corresponds to date of supply

Date	: 23.04.2009
Order No.	: RB09-6229
Offer No.	:
Customer No.	: 602200
Contact	: Julie Faust/Sn
Extension	: 07151 171610
E-Mail	: julie.faust@hoentzsch.com

Your Details:

Order	: CTS090385
Order Supplement	: ref: J van der Iaan
Contact	: Mrs. Tilly Spaans
Tel.	: 0031 174 272330
Fax	: 0031 174 272340
E-Mail	: Tilly.spaans@catec.nl
Requester	:
Supplier No.	:
Mode of Dispatch	: UPS
Dispatch No.	: j
Terms of Delivery	: EXW
VAT ID No.	: NL804250777B01

All Höntzsch products are in compliance with ElektroG, RoHS and WEEE according to EC Directive 2002/96/EC

Pos.	Article No. / Description	Quantity	Ordered	In arrears
1.	A000/400#000056 **HTA** Serial No.: 296	1	1	0
2.	B013/301#000076 **TA10-285GE 140/p16 ZG1b** Serial No.: ta120 3121 E 140°C	1	1	0
3.	KLB **ISO calibration certificate**	1	1	0

Höntzsch GmbH
Gottlieb-Daimler-Str. 37 · D-71334 Waiblingen
Fon +497151/1716-0 · Fax +497151/58402
info@hoentzsch.com · www.hoentzsch.com

Registergericht Stuttgart HRB 260 186
VAT-ID-Nr. DE 147322844
Geschäftsführer:
Thomas Itte · Dipl.-Ing. Uwe Steinhauser

Bankverbindungen:
Kreissparkasse · BLZ 602 500 10 · Konto 201 311
Volksbank · BLZ 602 901 10 · Konto 403 120 004
Dresdner Bank · BLZ 600 800 00 · Konto 341 770 000

höntzsch
flow measuring technology

[redacted]

Höntzsch GmbH Waiblingen

Kalibrierlabor für Strömungsgeschwindigkeit und Durchfluss von Gasen und Flüssigkeiten
Calibration laboratory for flow velocity and flow rate of gases and liquids

Kalibrierschein *Calibration Certificate*	Kalibrierscheinnummer *Number of Calibration Certificate*	09-6229-1

5. Messergebnisse
Measurement results

Referenz *Reference* m/s *(standard)*	Kalibriergegenstand *Calibration object* m/s *(standard)*	Abweichung *Deviation* m/s *(standard)*
2,00	1,99	-0,01
5,12	5,14	0,02
9,98	9,94	-0,04
40,08	39,87	-0,21
79,79	79,86	0,07
120,16	120,10	-0,06

6. Bemerkungen: Messunsicherheit bei Norm-Geschwindigkeiten
kleiner/gleich 40 m/s : 2 % v. M. + 0,02 m/s
größer 40 m/s : 2,5 % v. M.

Remarks *measurement uncertainty for standard velocity*
less than/equal to 40 m/s *: 2 % of measured value + 0.02 m/s*
greater than 40 m/s *: 2.5 % of measured value*

KKZ 0 4 9 3 C 8 3 7 B 7 5 7 7 5

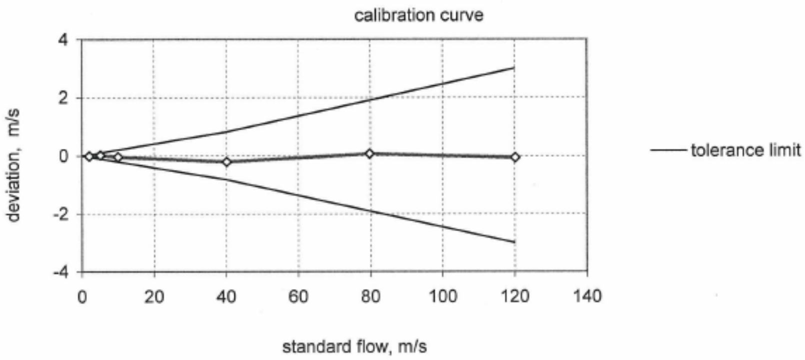

Appendix 3 Cross sections of welds

Weld depths at zero velocity and 4 kW. The mean depth equals 2.14 mm.

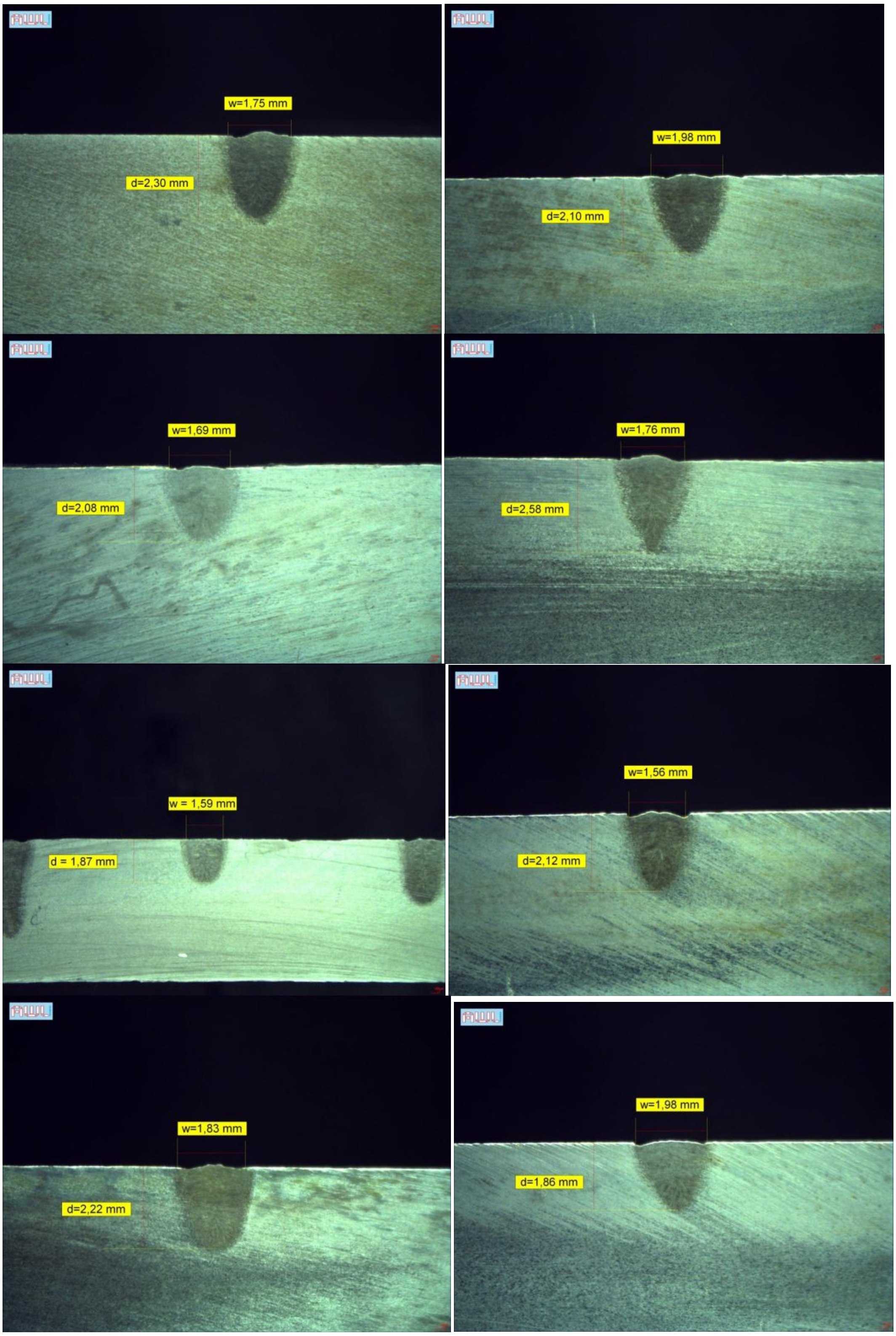

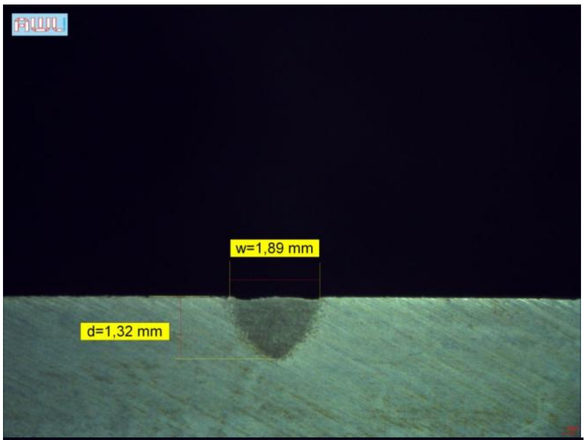
w=1,89 mm
d=1,32 mm
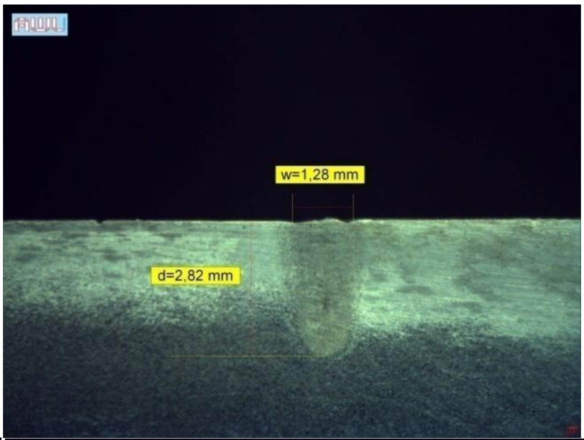
w=1,28 mm
d=2,82 mm
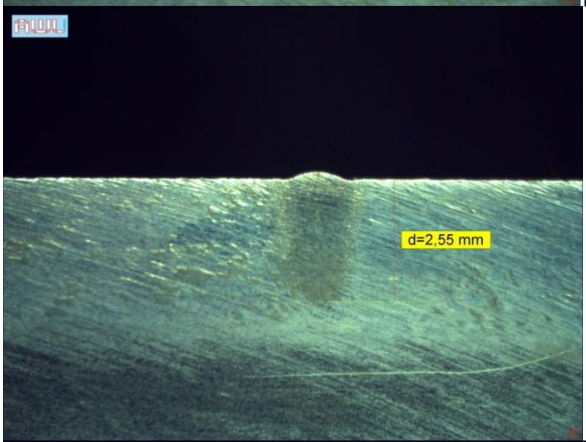
d=2,55 mm
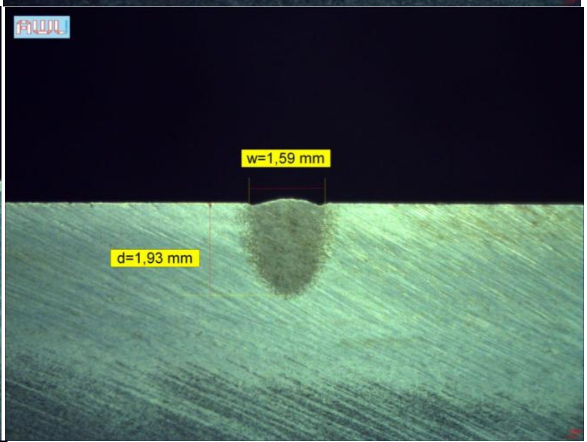
w=1,59 mm
d=1,93 mm
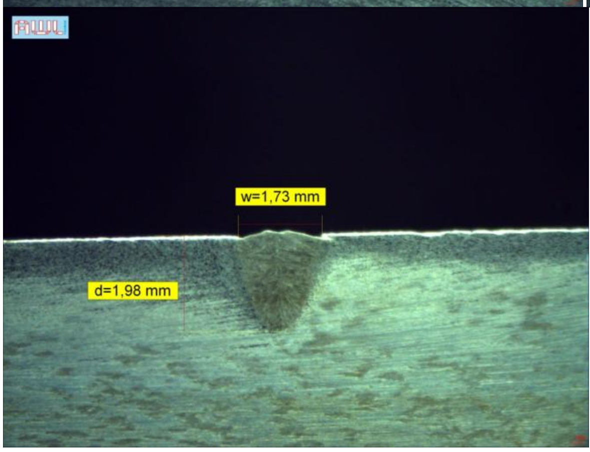
w=1,73 mm
d=1,98 mm
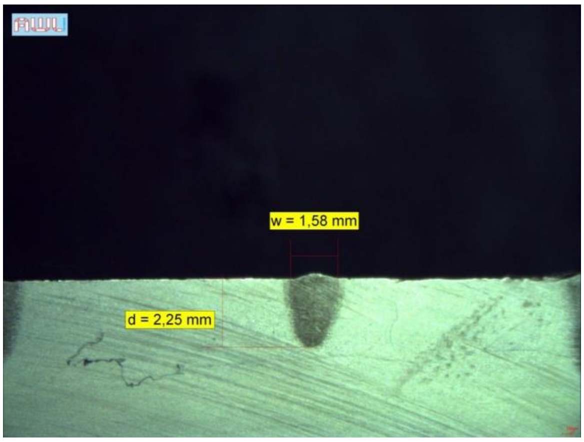
w = 1,58 mm
d = 2,25 mm

Weld depths at zero velocity and 6 kW. The mean depth equals 3.17 mm.

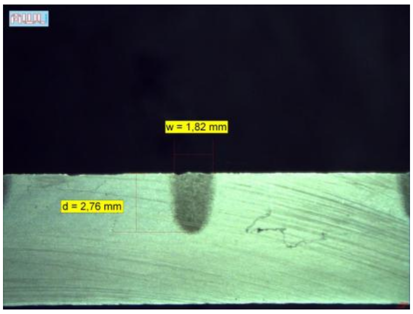

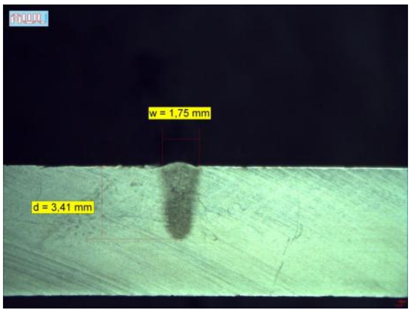

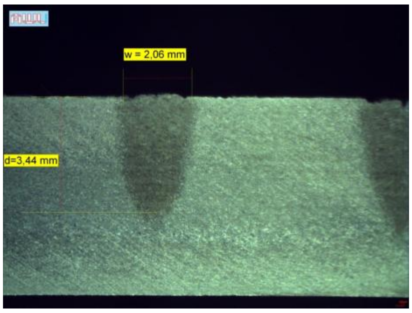

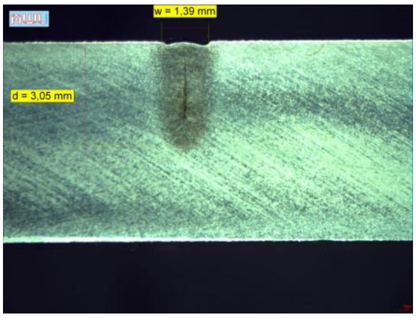

Cross sections at increasing air velocity at 4 kW. Air was blown using six nozzles in same direction as the weld direction. See Figure 27 for the d vs. V_{air} plot.

Vair= 3.2582 m/s

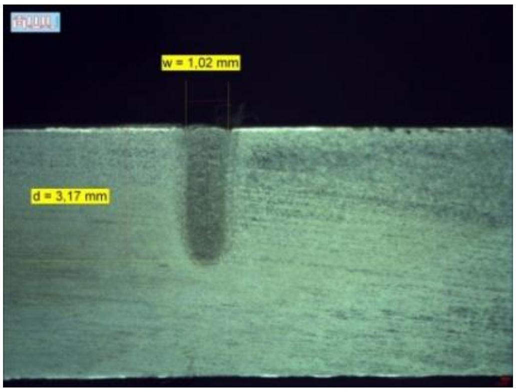

Vair= 3.9700 m/s

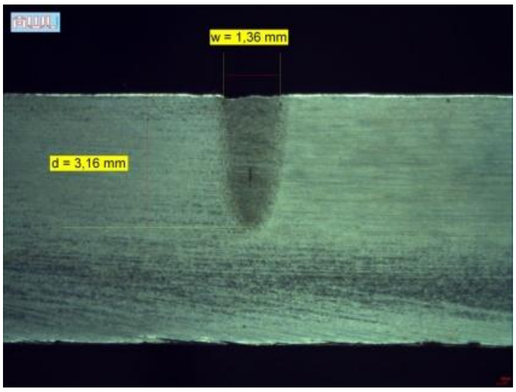

Vair= 4.5264 m/s

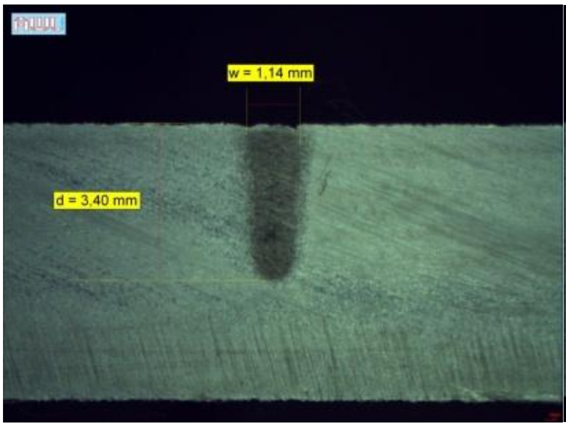

Vair= 5.0000 m/s

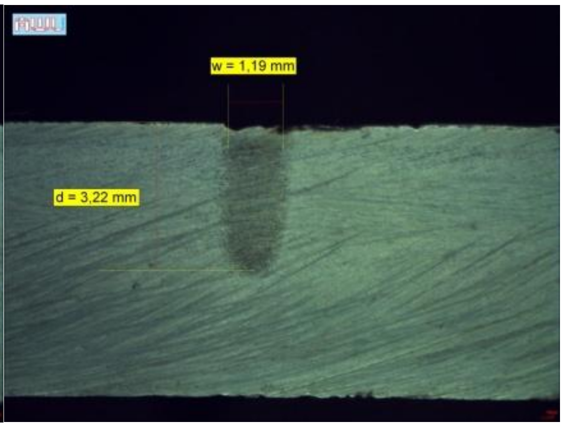

Vair= 5.8564 m/s

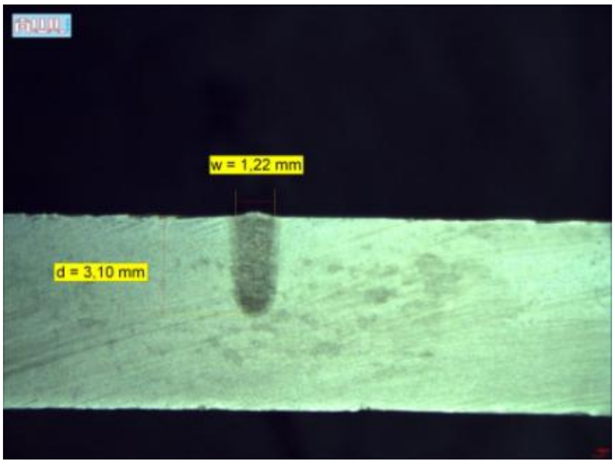

Cross sections at increasing air velocity at 6 kW. Air was blown using one nozzle in same direction as the weld direction. See Figure 25 for the d vs. V_{air} plot.

V_{air} = 1.06 m/s

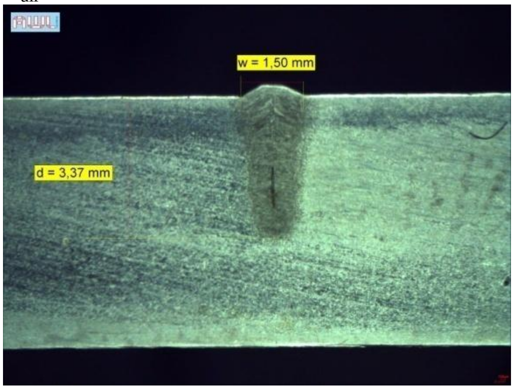

V_{air} = 2.27 m/s

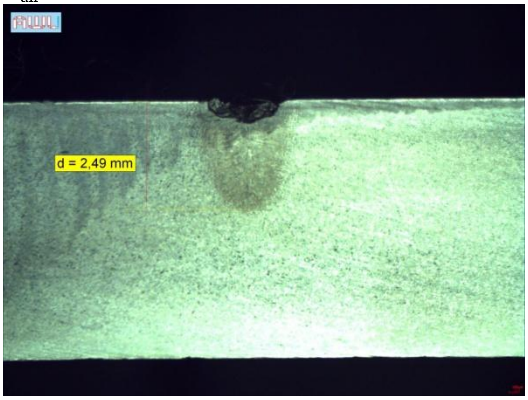

V_{air} = 3 m/s

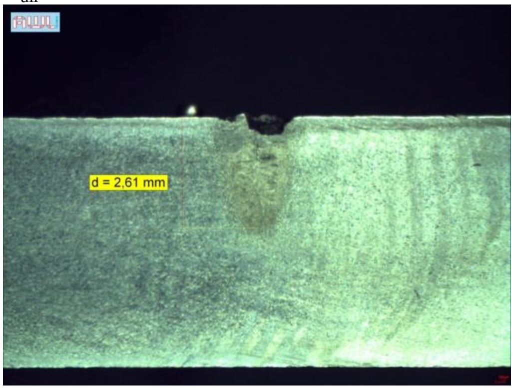

V_{air} = 3.85 m/s

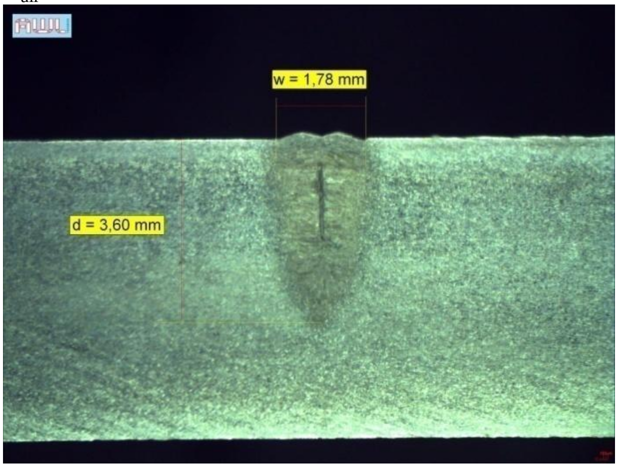

V_{air} = 4.99 m/s

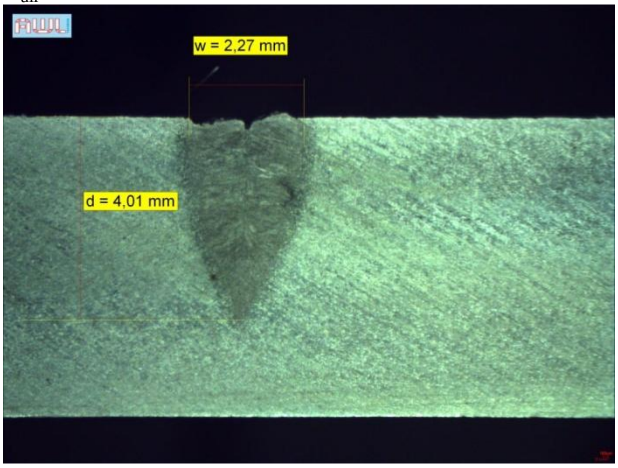

V_{air} = 6.36 m/s

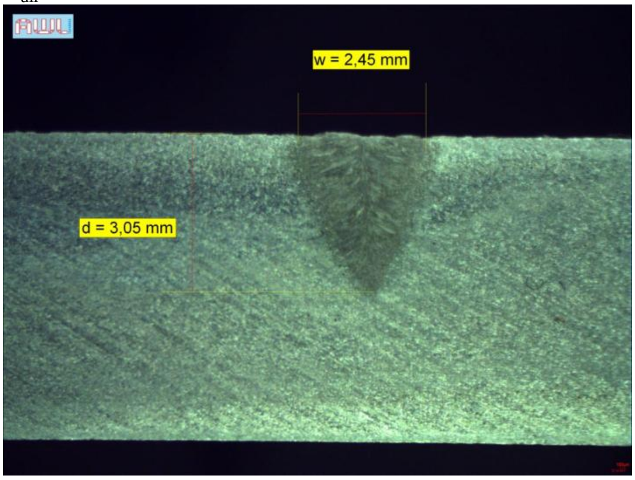

V_{air} = 9.9 m/s

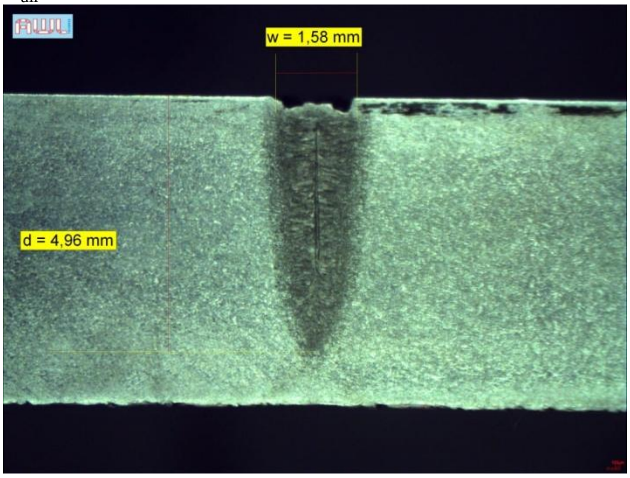

V_{air} = 19.73 m/s

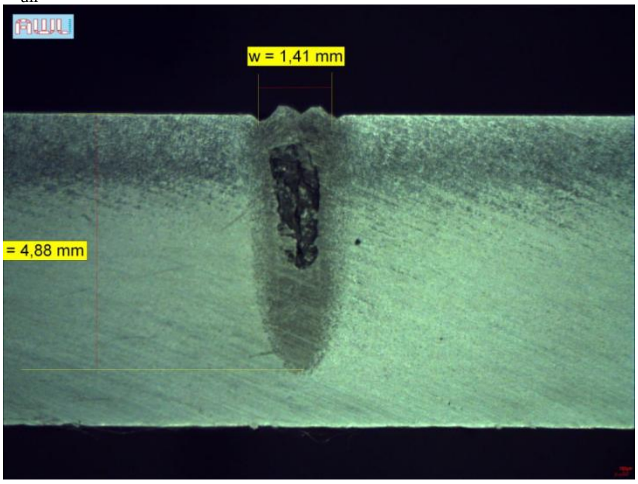

V_{air} = 25.67 m/s

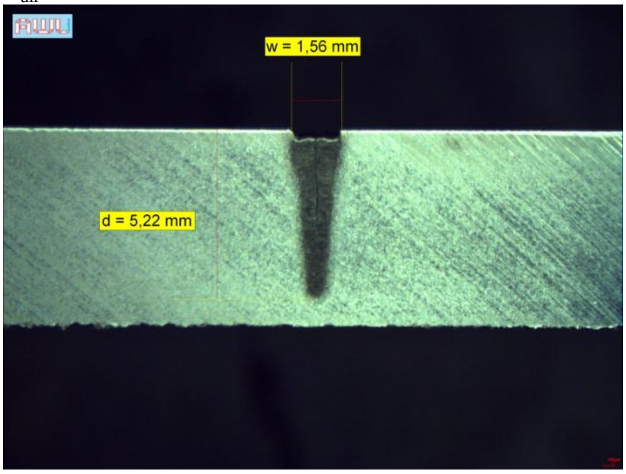

V_{air} = 32.25 m/s

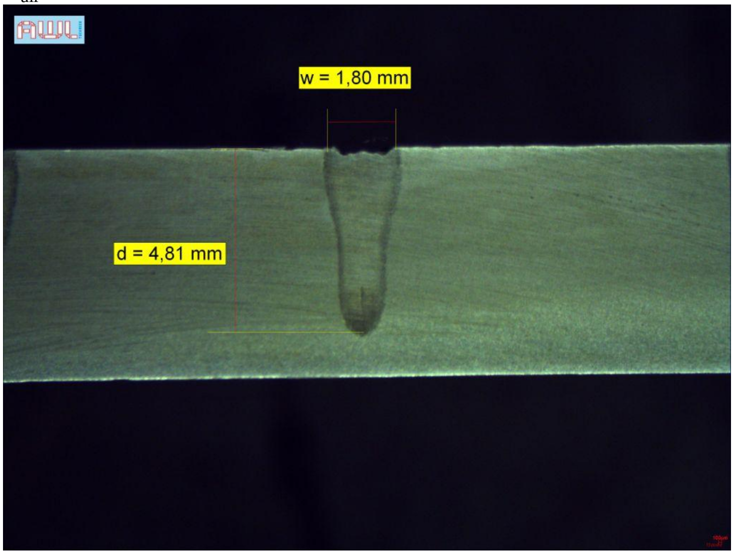

V_{air} = 35.94 m/s

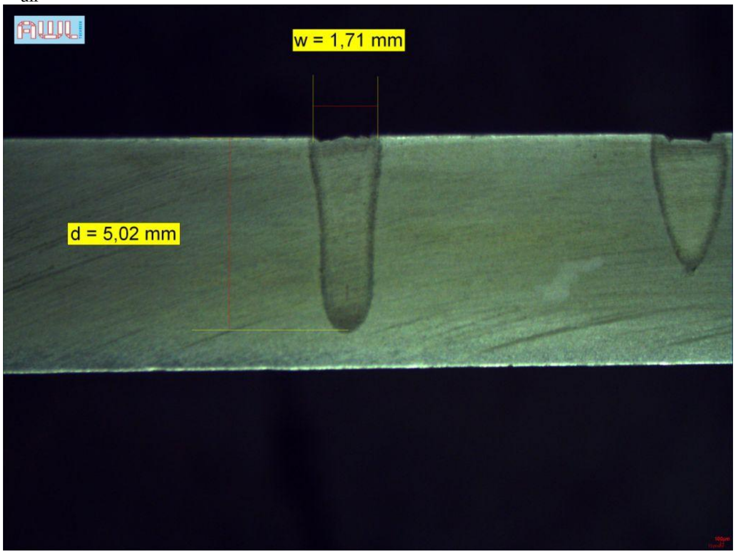

Appendix 4 RAPID (Robot programming code)

```
MODULE AirTestJetro

PROC rMainJetro()
        !
        r7LineTest;
        !r1LineTest;
        !
ENDPROC

PROC r1LineTest()

CONST laswelddata welddata1:= [50,500,0,0];
CONST robtarget pFirstPoint:= [[2097.84,-21.35,756.43],[0.00846848,0.705106,-0.709043,0.00347328],[-1,-2,0,1],[9E+09,9E+09,9E+09,9E+09,9E+09,9E+09]];
CONST AnyShapedata Line25mmOri := [[-11,0,0],[-10.5,0,0],[-
10,0,0],[[0,0,0],FALSE],[[0,0,0],FALSE],[[0,0,0],FALSE],[[0,0,0],FALSE],[[0,0,0],FALSE],[[0,0,0],FALSE],[[0,0,0],FALSE],[[0,0,0],FALSE],[[0,0,0],FALSE],[[0,0,0],FALSE],[[0,0,0],FALS
E],[[0,0,0],FALSE],[[0,0,0],FALSE],[[0,0,0],FALSE],[[0,0,0],FALSE],[[0,0,0],FALSE],[[0,0,0],FALSE],[[0,0,0],FALSE],[[0,0,0],FALSE],[[0,0,0],FALSE],[[0,0,0],FALSE],[[0,0,0],FALSE],[[
0,0,0],FALSE],[[0,0,0],FALSE],[[10,0,0],TRUE],[12.2,0,0],1,2,FALSE];

                rClearAllZone;
                !
                InitICAP;
                rInitLaser;
                rLaserTriggSetup;

                        IF OpMode()=OP_AUTO THEN
                        !
                        rLaserOn;
                        !
                        ENDIF

MoveAbsJ pR2HomeJoint,vMax,fine,tR2WeldGun;
LasAnyShape 1, pFirstPoint, welddata1, Line25mmOri\rot:=0, v2500, zAnyShape, tR2WeldGun;
MoveAbsJ pR2HomeJoint,vMax,fine,tR2WeldGun;

                Reset doFiberSelection1;
                Reset doFiberSelection2;
                !
                rLaserOff;
```

```
                    rLaserRequestOff;
ENDPROC

PROC r7LineTest()
          ! Declaratie van constanten.
                    CONST laswelddata welddata1:= [80,5000,0,0];![snelheid,vermogen,focus,0]
                    CONST laswelddata welddata2:= [80,5000,0,0];
                    CONST laswelddata welddata3:= [80,5000,0,0];
                    CONST laswelddata welddata4:= [80,5000,0,0];
                    CONST laswelddata welddata5:= [80,5000,0,0];
                    CONST laswelddata welddata6:= [80,5000,0,0];
                    CONST laswelddata welddata7:= [80,5000,0,0];
                    CONST laswelddata welddata8:= [80,5000,0,0];

CONST AnyShapedata shapedata_40_15:= [[-10,-7.6,0],[-10,-6.6,0],[-10,-5.6,0],[[-10,-0.6,0],TRUE],[[-8,1.4,0],TRUE],[[8,1.4,0],TRUE],[[10,-0.6,0],TRUE],[[10,-
4.6,0],TRUE],[[0,0,0],FALSE],[[0,0,0],FALSE],[[0,0,0],FALSE],[[0,0,0],FALSE],[[0,0,0],FALSE],[[0,0,0],FALSE],[[0,0,0],FALSE],[[0,0,0],FALSE],[[0,0,0],FALSE],[[0,0,0],FALSE],[[0,0,0]
,FALSE],[[0,0,0],FALSE],[[0,0,0],FALSE],[[0,0,0],FALSE],[[0,0,0],FALSE],[[0,0,0],FALSE],[[0,0,0],FALSE],[[0,0,0],FALSE],[[0,0,0],FALSE],[[0,0,0],FALSE],[10,-5.6,0],1,2,FALSE];
                    CONST AnyShapedata Line25mmOri := [[-11,0,0],[-10.5,0,0],[-
10,0,0],[[0,0,0],FALSE],[[0,0,0],FALSE],[[0,0,0],FALSE],[[0,0,0],FALSE],[[0,0,0],FALSE],[[0,0,0],FALSE],[[0,0,0],FALSE],[[0,0,0],FALSE],[[0,0,0],FALSE],[[0,0,0],FALSE],[[0,0,0],FALSE],[[0,0,0],FALS
E],[[0,0,0],FALSE],[[0,0,0],FALSE],[[0,0,0],FALSE],[[0,0,0],FALSE],[[0,0,0],FALSE],[[0,0,0],FALSE],[[0,0,0],FALSE],[[0,0,0],FALSE],[[0,0,0],FALSE],[[0,0,0],FALSE],[[0,0,0],FALSE],[[0,0,0],FALSE],[[
0,0,0],FALSE],[[0,0,0],FALSE],[[10,0,0],TRUE],[12.2,0,0],1,2,FALSE];
                    CONST AnyShapedata Line30mmOri := [[-16,0,0],[-15.5,0,0],[-
15,0,0],[[0,0,0],FALSE],[[0,0,0],FALSE],[[0,0,0],FALSE],[[0,0,0],FALSE],[[0,0,0],FALSE],[[0,0,0],FALSE],[[0,0,0],FALSE],[[0,0,0],FALSE],[[0,0,0],FALSE],[[0,0,0],FALSE],[[0,0,0],FALSE],[[0,0,0],FALS
E],[[0,0,0],FALSE],[[0,0,0],FALSE],[[0,0,0],FALSE],[[0,0,0],FALSE],[[0,0,0],FALSE],[[0,0,0],FALSE],[[0,0,0],FALSE],[[0,0,0],FALSE],[[0,0,0],FALSE],[[0,0,0],FALSE],[[0,0,0],FALSE],[[0,0,0],FALSE],[[
0,0,0],FALSE],[[0,0,0],FALSE],[[15,0,0],TRUE],[17,0,0],1,2,FALSE];
                    CONST AnyShapedata Line25mm := [[-11,0,0],[-10.5,0,0],[-10,0,0],[[-5.00,2.23,0],TRUE],[[0.00,0.00,0],TRUE],[[5.00,-
2.25,0],TRUE],[[0,0,0],FALSE],[[0,0,0],FALSE],[[0,0,0],FALSE],[[0,0,0],FALSE],[[0,0,0],FALSE],[[0,0,0],FALSE],[[0,0,0],FALSE],[[0,0,0],FALSE] ,[[0,0,0],FALSE],[[0,0,0],FALSE],[[0,0,0],FALSE],[[0,0,
0],FALSE],[[0,0,0],FALSE],[[0,0,0],FALSE],[[0,0,0],FALSE],[[0,0,0],FALSE],[[0,0,0],FALSE],[[0,0,0],FALSE],[[0,0,0],FALSE],[[0,0,0],FALSE],[[0,0,0],FALSE],[[0,0,0],FALSE],[[10,0,0],
TRUE],[12.2,0,0],1,2,FALSE];
                    CONST AnyShapedata Line5mmOri := [[-3.5,0,0],[-3,0,0],[-
2.5,0,0],[[0,0,0],FALSE],[[0,0,0],FALSE],[[0,0,0],FALSE],[[0,0,0],FALSE],[[0,0,0],FALSE],[[0,0,0],FALSE],[[0,0,0],FALSE],[[0,0,0],FALSE],[[0,0,0],FALSE],[[0,0,0],FALSE],[[0,0,0],FALSE],[[0,0,0],FAL
SE],[[0,0,0],FALSE],[[0,0,0],FALSE],[[0,0,0],FALSE],[[0,0,0],FALSE],[[0,0,0],FALSE],[[0,0,0],FALSE],[[0,0,0],FALSE],[[0,0,0],FALSE],[[0,0,0],FALSE],[[0,0,0],FALSE],[[0,0,0],FALSE],
[[0,0,0],FALSE],[[0,0,0],FALSE],[[2.5,0,0],TRUE],[4.5,0,0],1,2,FALSE];

                    CONST robtarget pFirstPoint:= [[2127.27,-21.61,756.42],[0.00125695,0.705103,-0.709095,-0.003688],[-1,-2,0,1],[9E+09,9E+09,9E+09,9E+09,9E+09,9E+09]];
                    !CONST robtarget pSecondPoint:= [[2127.27,-21.61,756.42],[0.00125695,0.705103,-0.709095,-0.003688],[-1,-2,0,1],[9E+09,9E+09,9E+09,9E+09,9E+09,9E+09]];
                    VAR Num J{1}:=[1];

                    ! Initialisatie van de Laser
                    rClearAllZone;
                    !
                    InitICAP;
                    rInitLaser;
```

```
		rLaserTriggSetup;
	!
		IF OpMode()=OP_AUTO THEN
			!
			rLaserOn;
			!
		ENDIF
		!
		! Robot beweging
			MoveAbsJ pR2HomeJoint,vMax,fine,tR2WeldGun;
			!v2500=snelheid waarmee robot naar het las toe beweegt
			LasAnyShape 1, pFirstPoint, welddata1, Line25mmOri\rot:=0, v2500, zAnyShape, tR2WeldGun\Wobj:=Wobj0;
			!
			LasAnyShape 2, reltool(offs(pFirstPoint,-10,0,0),0,0,0\Rx:=5)\refNormal:=pFirstPoint, welddata2, Line25mmOri\rot:=0, v2500, zAnyShape,
			tR2WeldGun\Wobj:=Wobj0;
			!
			LasAnyShape 3, reltool(offs(pFirstPoint,-20,0,0),0,0,0\Rx:=10)\refNormal:=pFirstPoint, welddata3, Line25mmOri\rot:=0, v2500, zAnyShape,
			tR2WeldGun\Wobj:=Wobj0;
			!
			LasAnyShape 4, reltool(offs(pFirstPoint,-30,0,0),0,0,0\Rx:=15)\refNormal:=pFirstPoint, welddata4, Line30mmOri\rot:=0, v2500, zAnyShape,
			tR2WeldGun\Wobj:=Wobj0;
			!
			LasAnyShape 5, reltool(offs(pFirstPoint,-40,0,0),0,0,0\Rx:=20)\refNormal:=pFirstPoint, welddata5, Line25mmOri\rot:=0, v2500, zAnyShape,
			tR2WeldGun\Wobj:=Wobj0;
			!
			LasAnyShape 6, reltool(offs(pFirstPoint,-50,0,0),0,0,0\Rx:=25)\refNormal:=pFirstPoint, welddata6, Line25mmOri\rot:=0, v2500, zAnyShape,
			tR2WeldGun\Wobj:=Wobj0;
			!
			LasAnyShape 7, reltool(offs(pFirstPoint,-60,0,0),0,0,0\Rx:=30)\refNormal:=pFirstPoint, welddata7, Line25mmOri\rot:=0, v2500, zAnyShape,
			tR2WeldGun\Wobj:=Wobj0;
			!
			MoveAbsJ pR2HomeJoint,vMax,fine,tR2WeldGun;

		! Uitzetten van de Laser
		Reset doFiberSelection1;
		Reset doFiberSelection2;
		!
		rLaserOff;
		rLaserRequestOff;
ENDPROC
ENDMODULE
```

Appendix 5 Matlab code

File 1: depth_at_zero_air_velocity.M

```
%% Mean depth at zero air velocity

% The first 5 elements of the array are for 'oppossite direction' case,
% the following 5 are for the 'same direction' case. And the last 4
elements
% are for 'perpendicular' case.
% For 4 kW the following experiments were used:
% experiment_2011_10_20_and_21_and_26_and_27. Also experiment 2011-11-8-3_5
% experiment 2011-11-8-3_5_7

d=[2.3;2.08;2.1;2.58;1.87;2.82;2.55;1.93;1.98;2.25;2.12;1.86;2.22;1.32];
d_average_4_kW=mean(d)

% For 6 kW the following experiments were used:
% 2011_11_8_3_6, 2011_11_8_3_8, 2011_11_10_2_9 and 2011_11_10_3_8
d=[3.05;3.44;2.76;3.41];
d_average_6_kW=mean(d)
```

File 2: one_nozzle_2_kW.m

```
%% One nozzle; 2kW; height=0/10/20/30 mm
%% Airflow perpendicular to weld direction

clear all;close all;clc;

% Previous name of file: experiment_2011_10_13_and_14
% Power=2 kW
% Airflow perpendicular to weld direction; Height=0
% Experiment: 2011_10_13_2

d_average_2_kW=(1.36+1.64+1.53)/3;% d_average_2_kW= 1.51;
% The average of only three welds is taken because the  weld depth at zero
% velocity of 2011-10-14-2 was unclear and not measured.

d            = [ 1.51,  0.83,   1.02,   1.22,   1.18, 1.02,     1.16];
V_measured   = [0,     1.39,   2.15,   3.03,   4.08,   5.16,   5.99];
axes('fontsize',25);
plot(V_measured,d,'-s','MarkerFaceColor','b');hold on;


% Airflow perpendicular to weld direction; Height=10
% Experiment: 2011_10_13_3

d            = [1.51, 1.17,   1.64,   1.52,   1.69,   1.51,   1.29];
V_measured   = [0,    1.1,    2.02,   3.14,   4.18,   5.18,   6.05];
plot(V_measured,d','-rs','MarkerFaceColor','r');hold on;


% Airflow perpendicular to weld direction; Height=20
% Experiment: 2011_10_14_1

d            =[ 1.51, 1.38,   1.52,   1.35,   1.2,    1.34,   1.28];
V_measured   =[0,    1.1,    2.21,   3.1,    4.07,   5.02,   6.05];
plot(V_measured,d,'-gs','MarkerFaceColor','g');hold on;


% Airflow perpendicular to weld direction; Height=30
% Experiment: 2011_10_14_2

d            =[1.51,    1.4,    1.65,   1.39,   1.26,   1.16,   1.03];
V_measured   =[0,    1.09,   2.19,   3.01,   4.04,   5.05,   6.08];
plot(V_measured,d,'-cs','MarkerFaceColor','c');hold on;
% Since d is unmeasurable at V_measured=0, d= average of all other depths
% when V_measured=o at different heights

ylim([0 6]);
legend({'h=0   mm','h=10 mm','h=20 mm','h=30 mm'});
xlabel({'V_{air} (m/s)'});ylabel('d (mm)');
title({'Airflow perpendicular to weld direction';'P = 2 kW';'V_{Laser} = 80
mm/s'});grid on;
```

File 3: one_nozzle_4_h_equals_0_10_20_30.m

```
%% One nozzle; 4kW; height=0/10/20/30 mm
%% Air blowing perpendicular,opposite and in same diriction as weld

close all;clear all; clc;

% Airflow opposite to weld direction; Height=0
% Experiment: 2011_10_20_1

d            = [2.1414;2.05;2.45;2.68;2.59;2.76;2.68];
V_measured   = [0;1.04;2.03;3.15;4.05;5.07;5.93];
axes('fontsize',25);plot(V_measured,d,'-s','MarkerFaceColor','b');hold on;

% Airflow opposite to weld direction; Height=10 mm
% Experiment: 2011_10_20_2

d            = [2.1414;2.96;3.24;3.03;2.69;2.75;2.89;];
V_measured   = [0;1.03;2.06;3.07;4.06;4.95;6.07];
plot(V_measured,d,'-rs','MarkerFaceColor','r');hold on;

% Airflow opposite to weld direction; Height=20 mm
% Experiment: 2011_10_21_1

d            = [2.1414;2.65;1.88;2.73;2.70;2.92;2.6];
V_measured   = [0;1.14;2.08;3.13;4.26;5.13;5.91];
plot(V_measured,d,'-gs','MarkerFaceColor','g');hold on;

% Airflow opposite to weld direction; Height=30 mm
% Experiment: 2011_10_21_2

d            = [2.1414;2.37;2.64;2.69;2.83;2.51;2.19;];
V_measured   = [0;1.05;2.05;2.98;4.07;5.05;5.98];
plot(V_measured,d,'-cs','MarkerFaceColor','c');hold on;

ylim([0 6]);
legend({'h=0   mm','h=10 mm','h=20 mm','h=30 mm'});
xlabel({'V_{air} (m/s)'});ylabel('d (mm)');
title({'Airflow opposite to weld direction';'P = 4 kW';'V_{Laser} = 80
mm/s'});grid on;

% Airflow parallel (same direction) as weld direction; Height=0 mm
% Experiment: 2011_10_26_1

figure(2);
d            = [2.1414;1.92;2.06;2.13;2.40;2.10;2.66;];
V_measured   = [0;1.32;2.18;3.36;4.09;5.3;6.16];
axes('fontsize',25);plot(V_measured,d,'-s','MarkerFaceColor','b');hold on;

% Airflow parallel (same direction) as weld direction; Height=10 mm
% Experiment: 2011_10_26_2

d            = [2.1414;1.73;2;2.2;2.21;3.07;3.24];
V_measured   = [0;1.19;2.15;3.15;4.18;5.06;6.25];
plot(V_measured,d,'-rs','MarkerFaceColor','r');hold on;

% Airflow parallel (same direction) as weld direction; Height=20 mm
% Experiment: 2011_10_26_3
```

```
d            = [2.1414;1.76;2.03;1.54;2.17;2.66;2.76];
V_measured  = [0;1.19;1.98;3.24;3.98;5.12;6.07];
plot(V_measured,d,'-gs','MarkerFaceColor','g');hold on;

% Airflow parallel (same direction) as weld direction; Height=30 mm
% Experiment: 2011_10_26_4

d            = [2.1414;2.01;2.05;2.49;2;1.86;2.08];
V_measured  = [0;1.1;2.07;3.2;4.07;5.22;5.98];
plot(V_measured,d,'-cs','MarkerFaceColor','c');hold on;

ylim([0 6]);
legend({'h=0   mm','h=10 mm','h=20 mm','h=30 mm'});
xlabel({'V_{air} (m/s)'});ylabel('d (mm)');
title({'Airflow in same direction as weld direction';'P = 4 kW';'V_{Laser}
= 80 mm/s'});grid on;

% Airflow perpendicular to weld direction; Height=0 mm
% Experiment: 2011_10_27_1

figure(3);
d            = [2.1414;2.27;2.03;2.46;2.59;2.38;2.38];
V_measured  = [0;1.19;1.90;3.33;4.15;5.17;6.16];
axes('fontsize',25);plot(V_measured,d,'-s','MarkerFaceColor','b');hold on;

% Airflow perpendicular to weld direction; Height=10 mm
% Experiment: 2011_10_27_2

d            = [2.1414;2.22;1.86;2.7;2.31;2.29;2.34];
V_measured  = [0;1.19;2.38;3.04;4.04;5.08;6.06];
plot(V_measured,d,'-rs','MarkerFaceColor','r');hold on;

% Airflow perpendicular to weld direction; Height=20 mm
% Experiment: 2011_10_27_3

d            = [2.1414;2.14;2.16;2.44;1.84;2.16;2.27];
V_measured  = [0;1.17;2.13;3.14;4.05;5.05;6.1];
plot(V_measured,d,'-gs','MarkerFaceColor','g');hold on;

% Airflow perpendicular to weld direction; Height=30 mm
% Experiment: 2011_10_27_4

d            = [2.1414;2.04;2.47;2.18;2.20;2.16;1.98;];
V_measured  = [0;1.1;2.05;3.02;4.14;5.04;6.09];
plot(V_measured,d,'-cs','MarkerFaceColor','c');hold on;

ylim([0 6]);
legend({'h=0   mm','h=10 mm','h=20 mm','h=30 mm'});
xlabel({'V_{air} (m/s)'});ylabel('d (mm)');
title({'Airflow perpendicular to weld direction';'P = 4 kW';'V_{Laser} = 80
mm/s'});grid on;
```

File 4: one_nozzle_4_and_6_kW_parallel_air_direction.m

```
%% One nozzle; 4 and 6 kW; height= 10 mm
%% Air direction parallel (opposite and same direction)

clear all;close all;clc;
%% Power= 4 kW and one nozzle

% Airflow opposite to weld direction; Height=10 mm
% Experiment: 2011_10_20_2 for 0-6 m/s
%             2011_11_10_1 for 10 and 20 m/s
%             2011_11_7_2  for 20-30 m/s

d           =
[2.1414;2.96;3.24;3.03;2.69;2.75;2.89;3.19;2.75;3.18;3.33;3.7];
V_measured  =
[0;1.03;2.06;3.07;4.06;4.95;6.07;10.24;19.73;27.73;29.14;31.8];
[c1,gof1] = fit(V_measured,d,'poly1')
axes('fontsize',22);
plot(V_measured,d,'s','MarkerFaceColor','b');hold on;plot(c1,'b');

% Airflow parallel (same direction) as weld direction; Height=10 mm
% Experiment: 2011_10_26_2 for 0-6 m/s
%             2011_11_10_1 for 10 and 20 m/s
%             2011_11_7_1  for 20-30 m/s


d           = [2.1414;1.73;2;2.2;2.21;3.07;3.24;4.1;4.17;3.48;2.86;3.51];
V_measured  = [0;1.19;2.15;3.15;4.18;5.06;6.25;9.9;19.73;28.7;32.25;35.94];
[c2,gof2] = fit(V_measured,d,'poly2')
plot(V_measured,d,'ro','MarkerFaceColor','r');hold on;plot(c2,'r');

ylim([0 6])
xlabel('V_{air} (m/s)');ylabel('d (mm)');
legend(' Opposite direction',' Linear fit \newline R^2=0.4047',' Same
direction',' 2^{nd} order polynomial fit \newline R^2=0.7584');
title({'Airflow parallel to weld direction using 1 nozzle';'P = 4
kW';'V_{Laser} = 80 mm/s'});grid on;


%% Power= 6 kW and one nozzle

% Airflow opposite to weld direction; Height=10 mm
% Experiment: 2011_11_10_3 for 0-6 m/s
%             2011_11_10_1 for 10 and 20 m/s
%             2011_11_7_2  for 20-30 m/s

d           =
[3.165;3.66;4.07;3.51;3.25;4.11;3.97;3.71;4.24;4.5;4.98;4.91];
V_measured  = [0;1.15;2.27;3;3.85;4.99;6.36;10.24;19.73;27.73;29.14;31.8];
[c3,gof3] = fit(V_measured,d,'poly1')
figure;
axes('fontsize',22);
plot(V_measured,d,'s','MarkerFaceColor','b');hold on;plot(c3,'b');

% Airflow parallel (same direction) as weld direction; Height=10 mm
% Experiment: 2011_11_10_2 for 0-6 m/s
%             2011_11_10_1 for 10 and 20 m/s
```

```
%             2011_11_7_1  for 20-30 m/s

d            =
[3.165;3.37;2.49;2.61;3.6;4.01;3.05;4.96;4.88;5.22;4.81;5.02];
V_measured  = [0;1.06;2.27;3;3.85;4.99;6.36;9.9;19.73;25.67;32.25;35.94];
[c4,gof4] = fit(V_measured(1:8),d(1:8),'poly1')
[c5,gof5] = fit(V_measured(9:12),d(9:12),'poly1')

plot(V_measured,d,'ro','MarkerFaceColor','r');hold on;plot(c4,'r');hold on;
plot(c5,'r');

ylim([0 6])
xlabel('V_{air} (m/s)');ylabel('d (mm)');
legend(' Opposite direction',' Linear fit \newline R^2=0.7681',' Same
direction',' Linear fit Sloping line \newline R^2=0.4868',' Linear fit Flat
line \newline R^2=0.0013');
title({'Airflow parallel to weld direction using 1 nozzle';'P = 6
kW';'V_{Laser} = 80 mm/s'});grid on;
```

File 5: six_nozzle_4_and_6_kW.m

```
%% Six nozzles; 4 and 6 kW
%% Air direction parallel (opposite and same direction)

clear all;clc;close all;
% 11 air measurements were done in the air profile above the weld.
% Also, the same amount of flow measurements were carried out.
% Lastly, the mean of these velocities and flow rates was determined
% ( see paragraph 3.2 of report)

%% Measurements carried out with 6 nozzles
% Experiment:
%
2011_11_7_3_and_2011_11_7_4_and_2011_11_8_1_and_2011_11_8_2_and_2011_11_8_3
(without
% mill)

% Mean of flow rate and velocity for experiment 2011_11_7_3
Sigma_v_1    =mean([143,148,150,138,134,144,150,139,148,141,152]);
V_air_1      =mean([5.93;0.24;5.31;1.1;4.87;1.16;4.38;0.69;6.06;0.21;5.89]);

% Mean of flow rate for experiment 2011_11_7_4
Sigma_v_2    =mean([186,192,177,188,184,179,179,184,189,189,188]);
V_air_2      =mean([6.9;0.45;6.38;1.88;5.9;1.44;4.89;2.22;5.36;1.16;7.09]);

% Mean of flow rate for experiment 2011_11_8_1
Sigma_v_3    =mean([208,196,200,201,211,208,195,196,201,204,208]);
V_air_3
=mean([7.73;0.74;7.72;2.19;6.72;2.15;5.94;2.14;5.52;1.47;7.47]);

% Mean of flow rate for experiment 2011_11_8_2
Sigma_v_4    =mean([222,227,220,210,228,221,224,221,223,215,220]);
V_air_4      =mean([8.37;0.99;8.49;2.46;6.87;2.15;6.02;3.13;6.6;1.5;8.42]);

% Mean of flow rate for experiment 2011_11_8_3
Sigma_v_5    =mean([245,241,262,255,257,260,263,251,251,242,242]);
V_air_5      =mean([10.05;1.12;9.8;2.44;8.61;2.74;7.71;3.39;7.7;1.4;9.46]);

% Measurements at 4 kW
% Opposite direction

d            = [2.1414;3.09;3.05;3.01;2.86;3.1];
V_air        = [0;V_air_1;V_air_2;V_air_3;V_air_4;V_air_5];
Sigma_v_measured=[Sigma_v_1;Sigma_v_2;Sigma_v_3;Sigma_v_4;Sigma_v_5];

[c1,gof1] = fit(V_air,d,'poly1')
axes('fontsize',22);plot(V_air,d,'s','MarkerFaceColor','b');hold
on;plot(c1,'b');hold on;

% Measurements at 4 kW
% Same direction

d            = [2.1414;3.17;3.16;3.40;3.22;3.1];
V_air        = [0;V_air_1;V_air_2;V_air_3;V_air_4;V_air_5];
Sigma_v_measured=[Sigma_v_1;Sigma_v_2;Sigma_v_3;Sigma_v_4;Sigma_v_5];

[c2,gof2] = fit(V_air,d,'poly1')
```

```
plot(V_air,d,'ro','MarkerFaceColor','r');hold on;plot(c2,'r')

xlim([0 6]);ylim([0 6]);

xlabel('V_{air} (m/s)');ylabel('d (mm)');
legend(' Opposite direction',' Linear fit \newline R^2=0.7341',' Same
direction',' Linear fit \newline R^2=0.7470');
title({'Airflow parallel to weld direction using 6 nozzles';'P = 4
kW';'V_{Laser} = 80 mm/s'});grid on;

% Measurements at 6 kW
% Opposite direction

d            = [3.1650;4.13;4.25;4.29;4.33;4.05];%d = [4.13;4.25;4.29;4.33];
V_air        = [0;V_air_1;V_air_2;V_air_3;V_air_4;V_air_5];
Sigma_v_measured=[Sigma_v_1;Sigma_v_2;Sigma_v_3;Sigma_v_4;Sigma_v_5];%Sigma
_v_measured=[Sigma_v_1;Sigma_v_2;Sigma_v_3;Sigma_v_4;];

[c3,gof3] = fit(V_air,d,'poly1')
figure;
axes('fontsize',22);plot(V_air,d,'s','MarkerFaceColor','b');hold
on;plot(c3,'b');hold on;

% Measurements at 6 kW
% Same direction

d            = [3.1650;4.16;4.33;4.11;4.10;4.16];
V_air        = [0;V_air_1;V_air_2;V_air_3;V_air_4;V_air_5];
Sigma_v_measured=[Sigma_v_1;Sigma_v_2;Sigma_v_3;Sigma_v_4;Sigma_v_5];

[c4,gof4] = fit(V_air,d,'poly1')
plot(V_air,d,'ro','MarkerFaceColor','r');hold on;plot(c4,'r');

xlim([0 6]);ylim([0 6])

xlabel('V_{air} (m/s)');ylabel('d (mm)');
legend(' Opposite direction',' Linear fit \newline R^2=0.7378',' Same
direction',' Linear fit \newline R^2=0.7319');
title({'Airflow parallel to weld direction using 6 nozzles';'P = 6
kW';'V_{Laser} = 80 mm/s'});grid on;
```